WILEY-VCH
Schowen
1. UK
N. Denzau

Kühn & Weyh Satz und Medien
Freiburg
l:/Vch/Schowen/3b2/c21.3d
19. 7. 2006

21
Dihydrogen Transfer and Symmetry: The Role of Symmetry in the Chemistry of Dihydrogen Transfer in the Light of NMR Spectroscopy

Gerd Buntkowsky and Hans-Heinrich Limbach

21.1
Introduction

The concept of symmetry is one of the basic pillars of modern chemistry and physics. Many fundamental phenomena and laws of nature are related to symmetry or are describable with the help of symmetry arguments. Accordingly, the mathematical description of symmetry, the so-called group theory, is at the heart of both classical mechanics and quantum mechanics. Since the latter field is the basis of modern chemistry, symmetry is also of great importance for chemists. They employ symmetry arguments on a regular basis to help in the understanding of spectra or molecular structures and courses on group theory are a regular part of the chemical education syllabus.

It is less well known that symmetry effects also play an important role in chemical kinetics, in particular when low mass particles like hydrogen or deuterium are involved in the reaction and quantum mechanical tunneling processes are present. Especially when dihydrogen exchange reactions are studied, the exchange of the two hydrogen atoms or more generally hydrons (i.e. ^{1}H, ^{2}H or ^{3}H) is a perfect symmetry operation. This apparently trivial symmetry has far fetching consequences for the reaction dynamics. These consequences stem from two different aspects of symmetry: On the one hand basic quantum mechanics tells us that the wavefunctions of the hydrogen or deuterium atoms have to obey the spin dependent Fermi symmetrization rules: They have to be either symmetric (deuterium, spin 1) or anti-symmetric (hydrogen, spin $^{1}/_{2}$). The result of this symmetrization is the formation of para- and ortho- states, which are the spin isotopomers of dihydrogen and dideuterium [1]. On the other hand group theory tells us that the eigenfunctions of the spatial Hamilton operator are now also eigenfunctions of the operator which exchanges the two hydrogen atoms. This implies that the eigenfunctions are either even or odd functions. As a consequence of this, the whole system behaves quantum mechanically. This is particularly visible at low temperatures when only the rotational ground states of the molecules are occupied.

Handbook of Hydrogen Transfer. Edited by R. L. Schowen

ISBN: 3-527-30777-X

WILEY-VCH
Schowen
1. UK
N. Denzau
Kühn & Weyh Satz und Medien
Freiburg
l:/Vch/Schowen/3b2/c21.3d
19. 7. 2006

These symmetry related quantum effects are most important in the chemistry of non-classical transition metal hydrides with η^2-bonded dihydrogen ligands [2–24]. Following the pioneering work of Kubas et al., who found the first of these complexes a whole series of transition metal polyhydrides with hydrogen distances varying between 0.8 and 1.7 Å were synthesized [23, 25–29]. Understanding their chemistry has led to a better understanding of catalysis since they may be catalytic precursors or stable models for short lived intermediate steps in catalysis [15, 30–32]. They are of current interest in organometallic chemistry [33–36].

Due to the η^2-binding the two hydrogen atoms forming the dihydrogen part of the system exhibit a much higher mobility than hydrogen atoms in conventional hydride bonds. In particular their exchange is an exact symmetry operation, as discussed above. The mutual exchange of the hydrons is equivalent to a hindered 180° rotation around the axis intersecting the M–H_2 angle [37–41]. The rotational barrier is caused mainly by the chemical structure, i.e. the binding between the two hydrogen atoms, the binding of the hydrons to the metal, effects of the ligands and sometimes also by crystal effects from neighboring molecules. For identical hydrogen isotopes, the above discussed quantum mechanical symmetry principles leads to the formation of para-states with anti parallel and ortho-states with parallel nuclear spins.

The various energy levels of the system exhibit a tunnel splitting and the energy eigenfunctions split into two separate manifolds with even and odd symmetry. The height of the barrier determines the energy difference between the lowest even and odd symmetry. This so-called tunnel splitting can be expressed as a tunnel frequency υ_t.

The size of the tunnel splitting depends strongly on the hindering potential. It varies from 10^{12} Hz for dihydrogen gas to a few Hz as the depth of the potential is increased. Due to this large range of tunnel frequencies no single spectroscopic technique is able to cover the whole dynamic range. While fast coherent tunneling in the frequency range of GHz to THz were studied by incoherent neutron scattering (INS) [19, 42], relatively slow tunneling processes in the frequency range of Hz to kHz are investigated by ^{1}H liquid state NMR spectroscopy (see for example Refs. [19, 43–49] and many others) or ^{2}H-liquid state NMR [50]. In these ^{1}H liquid state NMR studies the tunnel frequency is usually termed "quantum exchange coupling", due to the fact that the effect of the tunneling on the ^{1}H liquid state NMR spectra is equivalent to the effect of an indirect spin coupling (J-coupling). At higher temperatures incoherent exchange processes are superimposed on the coherent tunneling. They are also visible in the NMR or INS spectra of these hydrides.

An important application of these quantum mechanical symmetry principles is the so-called "Para Hydrogen Induced Polarization (PHIP)" experiments [51, 52]. If hydrogen gas (deuterium gas works similarly) is kept at low temperatures (typically liquid nitrogen or below), it converts after some time into the energetically favorable para-hydrogen, for example by contact with paramagnetic species [1] or adsorption to nuclear spins [53]. These para-hydrogen molecules are in a pure nuclear singlet state, which is associated via the Pauli exclusion principle with the

WILEY-VCH
Schowen
1. UK
N. Denzau
Kühn & Weyh Satz und Medien
Freiburg
l:/Vch/Schowen/3b2/c21.3d
19. 7. 2006

lowest rotational state. They are stable even in liquid solutions [54, 55]. Their high spin polarization can be utilized as an extremely sensitive monitor of the fate of the hydrogen in catalytically induced hydrogenation reactions (see for example Refs. [56–76]).

The rest of the paper is organized as follows: The second chapter gives an introduction into the theoretical description of tunneling phenomena and chemical kinetics. After a short summary about the connection of symmetry and tunneling, the basic properties of coherent and incoherent rotational tunneling and their relation to NMR spectroscopy are discussed and the empiric Bell [77] tunnel model is introduced, which is a powerful semi-empirical tool for the description of chemical kinetics in the transition from the coherent to the incoherent regime. This model has been used for the description of Arrhenius curves of H-transfers as described in more detail in Chapter 6. The next two chapters show applications of these symmetry effects. First the para-hydrogen induced polarization (PHIP) experiments are discussed. There the symmetry induced nuclear spin polarization creates very unconventional NMR lineshape patterns, which are of high diagnostic value for catalytic studies. Then in Section 21.4 symmetry effects on NMR lineshapes and relaxation data of intramolecular hydrogen exchange reactions are discussed and examples from ^{1}H-liquid state and ^{2}H-solid state NMR are presented and compared to INS spectra. The last section gives an outlook on possible future developments in the field.

21.2
Tunneling and Chemical Kinetics

This section gives an introduction to the effects of symmetry and quantum mechanical tunneling on chemical reactions in general and hydrogen transfer in particular.

21.2.1
The Role of Symmetry in Chemical Exchange Reactions

Starting from the early days of quantum mechanics, when the dynamics of the ammonia molecule was analyzed by Hund [78], it is well known that there is a close relationship between the symmetry of a potential and the wavefunction of the system [79]. The eigenfunctions of the system have the symmetry of the irreducible representations of the corresponding symmetry group. This situation gets particularly simple if one considers the motion in a symmetric double well potential, as for example in the case of ammonia, where the three hydrogen atoms can be either at the left or the right side of the nitrogen atom.

WILEY-VCH
Schowen
1. UK
N. Denzau

Kühn & Weyh Satz und Medien
Freiburg
l:/Vch/Schowen/3b2/c21.3d
19. 7. 2006

21.2.1.1 Coherent Tunneling

21.2.1.1.1 Tunneling in a Symmetric Double Minimum Potential

Basic textbook [80] quantum mechanics, already developed by Hund [78], tells us that we can associate two different wavefunctions $|1\rangle$ and $|2\rangle$ with these two states. Both have the same energy E_0. As long as the matrix element $H_{12} = \langle 1|\hat{H}|2\rangle = 0$ between these two states is zero, they are degenerate eigenstates of the system and this is the end of the story. The situation changes dramatically if $H_{12} \neq 0$, since then a level anti-crossing appears and $|1\rangle$ and $|2\rangle$ are no longer the eigenstates of the system. Instead the eigenfunctions are given by the symmetric (**g**erade) and anti-symmetric (**u**ngerade) linear combinations of $|1\rangle$ and $|2\rangle$.

$$|g\rangle = \frac{1}{\sqrt{2}}(|1\rangle + |2\rangle) \text{ and } |u\rangle = \frac{1}{\sqrt{2}}(|1\rangle - |2\rangle) \tag{21.1}$$

The corresponding energy levels are symmetrically split

$$E_k = E_0 \pm |H_{12}|. \tag{21.2}$$

The lower energy level belongs to the symmetric and the upper energy level to the anti-symmetric state.

Suppose now that we managed to prepare the system initially in the state $|1\rangle$. Since $|1\rangle$ is no longer an eigenstate of the system there is a periodic motion from $|1\rangle$ to $|2\rangle$ and back, where the probabilities of finding the system in state $|1\rangle$ and $|2\rangle$ change according to

$$p(1) = \cos^2(|H_{12}|t) \text{ and } p(2) = \sin^2(|H_{12}|t) \tag{21.3}$$

The frequency of this oscillation ν_t, the so-called tunnel frequency, is given via

$$\nu_t = \frac{2|H_{12}|}{2\pi} = \frac{|H_{12}|}{\pi} \tag{21.4}$$

This periodic motion is called the coherent tunneling of the system. It simply reflects the fact that the eigenstates of the system are given by Eq. (21.1). The size of the tunnel frequency depends strongly on the hindering potential.

21.2.1.1.2 Tunneling in a Symmetric Double Minimum Potential

In the case of dihydrogen exchange, a linear exchange of the two hydrons is not possible and angular degrees of freedom must be taken into account. Thus the simplest realistic model is a one-dimensional hindered rotation of the two hydrons around their center of mass in a harmonic twofold potential, i.e. a one-dimensional hindered quantum mechanical rotor. In this model it is assumed that the distance between the two hydrons, as well as their distance from the metal, does not change. In this case the angular position, described via an angle φ, is

WILEY-VCH
Schowen
1. UK
N. Denzau
Kühn & Weyh Satz und Medien
Freiburg
l:/Vch/Schowen/3b2/c21.3d
19. 7. 2006

used as the only degree of freedom. The corresponding Schrödinger equation of a rigid rotor in a harmonic twofold potential is:

$$-\frac{\hbar^2}{2\mu r^2}\frac{\mathrm{d}^2}{\mathrm{d}\varphi^2}|\Psi\rangle - V_0(1-\cos 2\varphi)|\Psi\rangle = E|\psi\rangle \tag{21.5}$$

where $2V_0$ describes the depth of the hindering potential and μ is the reduced mass of the hydrogen. This differential equation is of the Matthieu type.

For $V_0 = 0$ the dihydrogen is a free one-dimensional rotor with complex eigenfunctions of the type

$$|\Psi_k(\varphi)\rangle = \frac{1}{\sqrt{2\pi}}\exp(\mathrm{i}k\varphi) \text{ with } k = 0, \pm1, \pm2, \ldots \tag{21.6}$$

Since the corresponding energy eigenvalues

$$E_k = \frac{\hbar^2 k^2}{2mr^2} \tag{21.7}$$

are doubly degenerate $E_{+k} = E_{-k}$, we can use equally well their real and imaginary linear combinations, which are simple sine and cosine functions, respectively a constant ($k = 1, 2, \ldots$)

$$\begin{aligned}
|c_0(\varphi)\rangle &= \frac{1}{\sqrt{2\pi}} \\
|c_k(\varphi)\rangle &= \frac{1}{\sqrt{2}}(|\Psi_k(\varphi)\rangle + |\Psi_{-k}(\varphi)\rangle) = \frac{1}{\sqrt{\pi}}\cos(k\varphi) \\
|s_k(\varphi)\rangle &= \frac{1}{\sqrt{2}\mathrm{i}}(|\Psi_k(\varphi)\rangle - |\Psi_{-k}(\varphi)\rangle) = \frac{1}{\sqrt{\pi}}\sin(k\varphi)
\end{aligned} \tag{21.8}$$

They have even respectively odd symmetry with respect to φ:

$$|c_k(-\varphi)\rangle = |c_k(\varphi)\rangle \text{ and } |s_k(-\varphi)\rangle = -|s_k(\varphi)\rangle. \tag{21.9}$$

For $V_0 > 0$, they are no longer the eigenfunctions of the system. Employing them as base functions of the Hilbert space, the Schrödinger equation (21.5) is converted into a matrix equation, where the kinetic energy operator is diagonal and the only non-vanishing matrix elements are between even or odd,respectively, base functions which differ in the index k by ±2, i.e. $\langle c_0|\hat{V}|c_{\pm2}\rangle = \frac{1}{\sqrt{2}}V_0$ and

$$\begin{aligned}
\langle c_k|\hat{V}|c_l\rangle &= \frac{1}{2}V_0(\delta_{k,l+2} + \delta_{k,l-2}) \\
\langle s_k|\hat{V}|s_l\rangle &= \frac{1}{2}V_0(\delta_{k,l+2} + \delta_{k,l-2})
\end{aligned} \tag{21.10}$$

WILEY-VCH
Schowen
1. UK
N. Denzau

Kühn & Weyh Satz und Medien
Freiburg
l:/Vch/Schowen/3b2/c21.3d
19. 7. 2006

Thus the matrix is block diagonal and there are two sets of eigenfunctions, namely cosine type functions and sine type functions $|S_n(\varphi)\rangle$, which are linear combinations of the base functions (Eq. (21.9)

$$|C_n(\varphi)\rangle = \sum_{k=0}^{\infty} a_{n,k}|c_k(\varphi)\rangle \text{ and } |S_n(\varphi)\rangle = \sum_{k=1}^{\infty} b_{n,k}|s_k(\varphi)\rangle \tag{21.11}$$

The ground state wavefunction is always a cosine type state with even symmetry and the first excited state is always a sine type function with odd symmetry.

The energy differences between different $C_n(\varphi)$ or $S_n(\varphi)$ depend strongly on the depth of the potential $2V_0$ and vary between zero and the order of typical rotational μ wave or IR transitions (Fig. 21.2). At temperatures around 10 K only the lowest pair of eigenstates is thermally populated.

For identical hydrons, the symmetry postulate of identical particles has to be fulfilled. For protons and tritons this means that the overall wave function must be antisymmetric under particle exchange and for deuterons it must be symmetric under particle exchange. Due to this correlation of spin and spatial state, the energy difference ΔE between the lowest two spatial eigenstates can be treated as a pure spin Hamiltonian, similar to the Dirac exchange interaction of electronic spins.

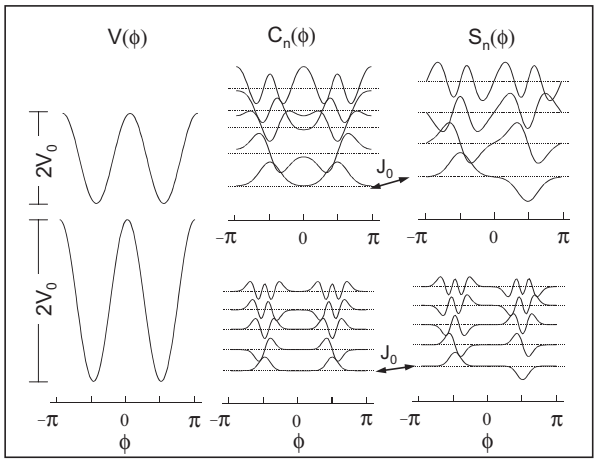

Figure 21.1 Eigenstates and energy eigenvalues of the Schrödinger equation of a rigid D_2 rotor in a harmonic twofold potential for two different depths of the potential barrier (adapted from Ref. [40]). Upper panel: $V_0 = 10^7$ MHz, $J_0 = 6.4 \times 10^3$ MHz, lower panel: $V_0 = 10^8$ MHz, $J_0 = 60$ Hz. Left : potential energy curve $V(\phi)$; middle panel : cosine type eigenfunctions $C_n(\phi)$, right panel: Sine type eigenfunctions $S_n(\phi)$. The energy shift between cosine and sine functions is increased artificially to demonstrate the differences in J_n between energy levels of same n.

WILEY-VCH
Schowen
1. UK
N. Denzau

Kühn & Weyh Satz und Medien
Freiburg
l:/Vch/Schowen/3b2/c21.3d
19. 7. 2006

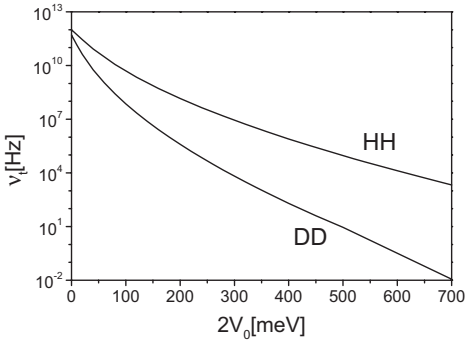

Figure 21.2 Tunnel frequency versus barrier [81]:Tunnel frequency and HH/DD isotope effect as a function of the barrier height $2V_0$ for a proton pair HH and a deuteron pair DD with $R_{DD} = 1$Å.

Spin 1/2 case: For a Spin $I = 1/2$ the eigenstates are

$$\begin{aligned} |S_0\rangle &= \frac{1}{\sqrt{2}}(|a\beta\rangle - |\beta a\rangle) \\ |T_{+1}\rangle &= |aa\rangle \\ |T_0\rangle &= \frac{1}{\sqrt{2}}(|a\beta\rangle + |\beta a\rangle) \\ |T_{+1}\rangle &= |\beta\beta\rangle \end{aligned} \tag{21.12}$$

The $|S_0\rangle$ state couples to the symmetric ground para-state to form a singlet manifold and the $|T_k\rangle$ states couple to the odd ortho-state and forms the triplet manifold. The splitting between these states is described by the quantum mechanical exchange interaction, which was given by Dirac in the form

$$\hat{H}_X = X\frac{1}{2}\left(1 + 4\hat{\vec{I}}_1\hat{\vec{I}}_2\right) \tag{21.13}$$

This Hamilton operator is the product of the energy splitting × times the operator

$$\hat{P} = \frac{1}{2}\left(1 + 4\hat{\vec{I}}_1\hat{\vec{I}}_2\right) = \begin{pmatrix} 1 & 0 & 0 & 0 \\ 0 & 0 & 1 & 0 \\ 0 & 1 & 0 & 0 \\ 0 & 0 & 0 & 1 \end{pmatrix} \tag{21.14}$$

Permutation operator: The operator $\hat{P}$ is an example of a permutation operator in spin space. It exchanges the coordinates of the two spins 1/2. In the product space

WILEY-VCH
Schowen
1. UK
N. Denzau

Kühn & Weyh Satz und Medien
Freiburg
l:/Vch/Schowen/3b2/c21.3d
19. 7. 2006

of the two spins the general definition of such an operator for arbitrary spins is given via

$$\hat{P}\left(\hat{\vec{I}}_1, \hat{\vec{I}}_2\right)|\mu, \nu\rangle = |\nu, \mu\rangle \tag{21.15}$$

An very useful alternate representation of the operator $\hat{P}$ is found if symmetry adapted base functions $|\lambda\rangle$ are employed. In this base the permutation operator is diagonal with diagonal elements $+1$ if the state has even and -1 if the state has odd symmetry.

$$\hat{P}\left(\hat{\vec{I}}_1, \hat{\vec{I}}_2\right)|\lambda\rangle = \pm|\lambda\rangle \tag{21.16}$$

Employing these permutation operators it is easy to write down the exchange Hamiltonian for arbitrary spins.

From the NMR point of view, the eigenfunctions of the spin $^1/_2$ exchange Hamiltonian are identical to the eigenfunctions of the "normal" homonuclear spin–spin interaction, but the energy eigenvalues are shifted by a constant offset of $X/2$, since

$$\begin{aligned}\hat{H}_X &= \frac{X}{2} + 2X\hat{\vec{I}}_1\hat{\vec{I}}_2 \\ &= \frac{X}{2} + J_X\hat{\vec{I}}_1\hat{\vec{I}}_2\end{aligned} \tag{21.17}$$

Thus for spin $I = 1/2$ nuclei, the quantum mechanical exchange interaction is formally equivalent to an indirect spin–spin interaction. Accordingly the exchange of spin-1/2 particle is usually treated in NMR like a J-coupling (quantum exchange coupling), employing the more simple Hamiltonian

$$\hat{H}'_X = J_X\hat{\vec{I}}_1\hat{\vec{I}}_2 \tag{21.18}$$

These couplings are indeed directly visible in liquid state ^{1}H-NMR spectra [46, 47].

Spin 1 case: For a Spin $I = 1$ the nine eigenstates of a di-deuterium system are

$$\begin{aligned}
&|a_1\rangle = |{+}{+}\rangle \qquad |a_2\rangle = |00\rangle \qquad |a_3\rangle = |{-}{-}\rangle \\
&|a_4\rangle = \frac{1}{\sqrt{2}}(|{+}{-}\rangle + |{-}{+}\rangle) \qquad |a_5\rangle = \frac{1}{\sqrt{2}}(|{+}0\rangle + |0{+}\rangle) \qquad |a_6\rangle = \frac{1}{\sqrt{2}}(|{-}0\rangle + |01\rangle) \\
&|b_1\rangle = \frac{1}{\sqrt{2}}(|{+}{-}\rangle - |{-}{+}\rangle) \qquad |b_2\rangle = \frac{1}{\sqrt{2}}(|{+}0\rangle - |0{+}\rangle) \qquad |b_3\rangle = \frac{1}{\sqrt{2}}(|{-}0\rangle - |01\rangle)
\end{aligned} \tag{21.19}$$

The three *b*-states have odd and the six *a*-states have even symmetry. Since the deuterium nucleus is a boson, the overall wavefunction has to be symmetric and

WILEY-VCH
Schowen
1. UK
N. Denzau
Kühn & Weyh Satz und Medien
Freiburg
l:/Vch/Schowen/3b2/c21.3d
19. 7. 2006

the six even *a*-states couple to the even ground state and the three odd *b*-states couple to the odd spatial state. The special form of the operator $\hat{P}$ is calculated from Eq. (21.15) or (21.16). For arbitrary base sets, a base independent operator representation of the permutation operator of spin 1 similar to the spin $^1/_2$ case of Eq. (21.18) is useful. This representation can be found with the help of the following set of normalized single spin operators:

$$
\begin{aligned}
B_1 &= \frac{1}{\sqrt{2}} S_x & B_2 &= \frac{1}{\sqrt{2}} S_y \\
B_3 &= \frac{1}{\sqrt{2}} S_z & B_4 &= \frac{1}{\sqrt{2}} E \\
B_5 &= \frac{1}{2}\sqrt{6}\left(S_z^2 - \frac{2}{3} \right) & B_6 &= \frac{1}{\sqrt{2}}\left(S_y^2 - S_x^2 \right) \\
B_7 &= \frac{1}{\sqrt{2}}\left(S_x S_y + S_y S_x \right) & B_8 &= \frac{1}{\sqrt{2}}(S_x S_z + S_z S_x) \\
B_9 &= \frac{1}{\sqrt{2}}\left(S_y S_z + S_z S_y \right)
\end{aligned}
\tag{21.20}
$$

Employing these base operators the permutation operator of a homo nuclear spin 1 pair is given by

$$
\hat{P}\left(\hat{\vec{I}}_1, \hat{\vec{I}}_2 \right) = \sum_k B_k \otimes B_k \tag{21.21}
$$

where $\otimes$ denotes the tensor or direct product of two vector spaces (see for example Refs. [80, 82]).

As a result we find that in both the hydrogen and the deuterium case the ground state tunneling is describable by a pure spin tunnel Hamiltonian, which describes the tunnel splitting between the spatial pair of states of different symmetry. The implications are discussed in detail in Ref. [83].

Coherent tunneling at higher temperatures: If several pairs of tunnel levels are thermally populated, the thermal average of the different pairs of tunnel levels has to be calculated. As long as only a few levels far below the barrier are contributing, the values of the various tunnel frequencies $J_n = \nu_{tn}$ will be small compared to the thermal exchange rates between the level pairs and the averaging can be done by summing up the individual values of ν_{tn} times their thermal population. This averaging can be approximated using the population of one of the connected levels:

$$
\nu_t = \sum_n \nu_{tn} \exp\left(-\frac{E_n}{kT} \right) \tag{21.22}
$$

The situation becomes more difficult if the values of ν_t are comparable or greater than the thermal population rates or decay rates. In this regime, a transition from coherent to incoherent exchange will take place, as shown below, as was shown by density matrix theory [19].

WILEY-VCH
Schowen
1. UK
N. Denzau

Kühn & Weyh Satz und Medien
Freiburg
l:/Vch/Schowen/3b2/c21.3d
19. 7. 2006

21.2.1.2 The Density Matrix

As soon as large ensembles of particles with statistical populations of the eigenstates and incoherent exchange and relaxation processes between these states are investigated, quantum statistical tools are necessary to describe the system. In this situation the quantum mechanical density operator $\hat{\rho}$ has to be employed. For the coherent evolution of the density operator under the influence of a Hamiltonian $\hat{H}$, the following differential equation is found [80]

$$\frac{\mathrm{d}}{\mathrm{d}t}\hat{\rho} = -\mathrm{i}\left[\hat{H}, \hat{\rho}\right] \tag{21.23}$$

In this equation we have followed the NMR convention and set the constant $\hbar = 1$. This is equivalent to measuring energies in angular frequency units. Employing a suitable set of base functions of the Hilbert space, this equation can be converted into a set of linear differential equations for the matrix elements of $\hat{\rho}$. In the case of a single pair of tunnel levels the Hamiltonian of the two levels with their tunnel splitting can be treated as a two-level system, employing fictitious spin 1/2 operators, describable by the Hamiltonian $\hat{H}$

$$\begin{aligned}\hat{H} &= \begin{pmatrix} E_1 & 0 \\ 0 & E_2 \end{pmatrix} = \frac{E_1 + E_2}{2}\begin{pmatrix} 1 & 0 \\ 0 & 1 \end{pmatrix} + \frac{E_1 - E_2}{2}\begin{pmatrix} 1 & 0 \\ 0 & -1 \end{pmatrix} \\ &= \frac{E_1 + E_2}{2} + (E_1 - E_2)\hat{S}_z = E + \nu_t \hat{S}_z\end{aligned} \tag{21.24}$$

Here $E = \dfrac{E_1 + E_2}{2}$ is the mean energy of the levels and $\nu_t = (E_1 - E_2)$ is the tunnel frequency. This set of differential equations is most conveniently written by introducing the so-called Liouville super operator $\hat{\hat{L}}$, which defines the Liouville space, where the density matrix becomes a vector. The equation of motion of the density matrix is

$$\frac{\mathrm{d}}{\mathrm{d}t}\hat{\rho} = -\mathrm{i}\hat{\hat{L}}\hat{\rho} \tag{21.25}$$

The Liouville operator is constructed from the Hamiltonian via

$$\hat{\hat{L}} = \hat{H} \otimes \hat{\hat{E}} - \hat{E} \otimes \hat{\hat{H}} \tag{21.26}$$

Here, $\hat{E}$ is the unity matrix of Hilbert space. In the case of the tunnel Hamiltonian it is simply

$$\hat{\hat{L}} = \nu_t \hat{\hat{S}}_z = \nu_t \begin{pmatrix} 0 & 0 & 0 & 0 \\ 0 & 1 & 0 & 0 \\ 0 & 0 & -1 & 0 \\ 0 & 0 & 0 & 0 \end{pmatrix} \tag{21.27}$$

WILEY-VCH
Schowen
1. UK
N. Denzau

Kühn & Weyh Satz und Medien
Freiburg
l:/Vch/Schowen/3b2/c21.3d
19. 7. 2006

21.2.1.3 The Transition from Coherent to Incoherent Tunneling

A rigorous quantum mechanical theory of the transition from coherent to incoherent tunneling was developed by Szymanski [84] and Scheurer [85]. The results of this elaborate theory can be reproduced by a combination of density matrix theory and formal kinetics as was shown in Ref. [19].

The transition from coherent to incoherent tunneling is most easily understood by considering the ground state of the system and the first excited state. In the systems under consideration the typical energy difference between the ground state and the first excited state is in the range 40–50 meV. At temperatures below 50 K practically only the ground state is populated ($n_b < 10^{-5} n_a$) and only a small population is found in the excited state.

As a starting point let us see what happens, if we consider not only the ground state, but also the first excited state of the tunneling pairs. Both states are connected via thermal excitation with rates k_{ab} and k_{ba}. Since the transition between even and odd states is both symmetry and spin forbidden, these rates connect only states of the same symmetry and the spin is conserved in the transition. From the principle of detailed balance we find for the ratio of the rates

$$\frac{k_{ab}}{k_{ba}} = \exp\left(-\frac{E_b - E_a}{k_B T}\right) << 1 \tag{21.28}$$

The coherent evolution of the density matrix is described by the corresponding Liouville operators:

$$\hat{\hat{L}}_a = \upsilon_{ta} \begin{pmatrix} 0 & 0 & 0 & 0 \\ 0 & 1 & 0 & 0 \\ 0 & 0 & -1 & 0 \\ 0 & 0 & 0 & 0 \end{pmatrix} \text{ and } \hat{\hat{L}}_b = \upsilon_{tb} \begin{pmatrix} 0 & 0 & 0 & 0 \\ 0 & 1 & 0 & 0 \\ 0 & 0 & -1 & 0 \\ 0 & 0 & 0 & 0 \end{pmatrix} \tag{21.29}$$

The exchange between the levels connects the two Liouville spaces

$$\begin{aligned} \frac{\mathrm{d}}{\mathrm{d}t}\hat{\rho}_a &= -(k_{ab} + iL_a)\hat{\rho}_a + k_{ba}\hat{\rho}_b \\ \frac{\mathrm{d}}{\mathrm{d}t}\hat{\rho}_b &= -(k_{ba} + iL_b)\hat{\rho}_b + k_{ab}\hat{\rho}_a \end{aligned} \tag{21.30}$$

In matrix form these coupled differential equations are

$$\frac{\mathrm{d}}{\mathrm{d}t}\begin{pmatrix} \rho_{a1} \\ \rho_{a2} \\ \rho_{a3} \\ \rho_{a4} \end{pmatrix} = \begin{pmatrix} -k_{ab} & 0 & 0 & 0 \\ 0 & -k_{ab} - \mathrm{i}\upsilon_{ta} & 0 & 0 \\ 0 & 0 & -k_{ab} + \mathrm{i}\upsilon_{ta} & 0 \\ 0 & 0 & 0 & -k_{ab} \end{pmatrix} \begin{pmatrix} \rho_{a1} \\ \rho_{a2} \\ \rho_{a3} \\ \rho_{a4} \end{pmatrix} + k_{ba} \begin{pmatrix} \rho_{b1} \\ \rho_{b2} \\ \rho_{b3} \\ \rho_{b4} \end{pmatrix} \tag{21.31}$$

WILEY-VCH
Schowen
1. UK
N. Denzau

Kühn & Weyh Satz und Medien
Freiburg
l:/Vch/Schowen/3b2/c21.3d
19. 7. 2006

and

$$\frac{\mathrm{d}}{\mathrm{d}t}\begin{pmatrix}\rho_{b1}\\ \rho_{b2}\\ \rho_{b3}\\ \rho_{b4}\end{pmatrix} = \begin{pmatrix}-k_{ba} & 0 & 0 & 0\\ 0 & -k_{ba}-\mathrm{i}\upsilon_{tb} & 0 & 0\\ 0 & 0 & -k_{ba}+\mathrm{i}\upsilon_{tb} & 0\\ 0 & 0 & 0 & -k_{ba}\end{pmatrix}\begin{pmatrix}\rho_{b1}\\ \rho_{b2}\\ \rho_{b3}\\ \rho_{b4}\end{pmatrix} + k_{ab}\begin{pmatrix}\rho_{a1}\\ \rho_{a2}\\ \rho_{a3}\\ \rho_{a4}\end{pmatrix} \tag{21.32}$$

This system of equations can be greatly simplified by the fact that the excited state is only weakly populated. This allows us to use a quasi-stationary condition for the excited state by setting the derivative of the population of the excited state to zero. This converts the second differential equation into an algebraic one.

$$\begin{pmatrix}-k_{ba} & 0 & 0 & 0\\ 0 & -k_{ba}-\mathrm{i}\upsilon_{tb} & 0 & 0\\ 0 & 0 & -k_{ba}+\mathrm{i}\upsilon_{tb} & 0\\ 0 & 0 & 0 & -k_{ba}\end{pmatrix}\begin{pmatrix}\rho_{b1}\\ \rho_{b2}\\ \rho_{b3}\\ \rho_{b4}\end{pmatrix} + k_{ab}\begin{pmatrix}\rho_{a1}\\ \rho_{a2}\\ \rho_{a3}\\ \rho_{a4}\end{pmatrix} = 0 \tag{21.33}$$

Solving for ρ_b gives:

$$\begin{pmatrix}\rho_{b1}\\ \rho_{b2}\\ \rho_{b3}\\ \rho_{b4}\end{pmatrix} = \begin{pmatrix}\frac{k_{ab}}{k_{ba}}\rho_{a1}\\ \frac{k_{ab}}{k_{ba}+\mathrm{i}\upsilon_{tb}}\rho_{a2}\\ \frac{k_{ab}}{k_{ba}-\mathrm{i}\upsilon_{tb}}\rho_{a3}\\ \frac{k_{ab}}{k_{ba}}\rho_{a4}\end{pmatrix} \tag{21.34}$$

Inserting this expression into the equation for ρ_a gives after some simple manipulations:

$$\frac{\mathrm{d}}{\mathrm{d}t}\begin{pmatrix}\rho_{a1}\\ \rho_{a2}\\ \rho_{a3}\\ \rho_{a4}\end{pmatrix} = \begin{pmatrix}0 & 0 & 0 & 0\\ 0 & -k_{ab}-\mathrm{i}\upsilon_{ta}+\frac{k_{ab}k_{ba}}{k_{ba}+\mathrm{i}\upsilon_{tb}} & 0 & 0\\ 0 & 0 & -k_{ab}+\mathrm{i}\upsilon_{ta}+\frac{k_{ab}k_{ba}}{k_{ba}-\mathrm{i}\upsilon_{tb}} & 0\\ 0 & 0 & 0 & 0\end{pmatrix}\begin{pmatrix}\rho_{a1}\\ \rho_{a2}\\ \rho_{a3}\\ \rho_{a4}\end{pmatrix} \tag{21.35}$$

From the first and the last row it is evident that the density matrix elements ρ_{a1} and ρ_{a4}, which correspond to the populations of the levels, do not change. The center rows become:

$$\frac{\mathrm{d}}{\mathrm{d}t}\rho_{a2} = \left(-k_{ab}-\mathrm{i}\upsilon_{ta}+\frac{k_{ab}k_{ba}}{k_{ba}+\mathrm{i}\upsilon_{tb}}\right)\rho_{a2} \tag{21.36}$$

and

$$\frac{\mathrm{d}}{\mathrm{d}t}\rho_{a3} = \left(-k_{ab}+\mathrm{i}\upsilon_{ta}+\frac{k_{ab}k_{ba}}{k_{ba}-\mathrm{i}\upsilon_{tb}}\right)\rho_{a3} \tag{21.37}$$

WILEY-VCH
Schowen
1. UK
N. Denzau

Kühn & Weyh Satz und Medien
Freiburg
l:/Vch/Schowen/3b2/c21.3d
19. 7. 2006

They can be rewritten as

$$\frac{\mathrm{d}}{\mathrm{d}t}\,\rho_{a2} = \left(-\left(\frac{k_{ab}\upsilon_{tb}^2}{k_{ba}^2+\upsilon_{tb}^2}\right) - i\left(\upsilon_{ta} + \frac{k_{ab}k_{ba}}{k_{ba}^2+\upsilon_{tb}^2}\,\upsilon_{tb}\right)\right)\rho_{a2} \tag{21.38}$$

and

$$\frac{\mathrm{d}}{\mathrm{d}t}\,\rho_{a3} = \left(-\left(\frac{k_{ab}\upsilon_{tb}^2}{k_{ba}^2+\upsilon_{tb}^2}\right) + i\left(\upsilon_{ta} + \frac{k_{ab}k_{ba}}{k_{ba}^2+\upsilon_{tb}^2}\,\upsilon_{tb}\right)\right)\rho_{a3} \tag{21.39}$$

The density matrix elements ρ_{a2} and ρ_{a3} represent coherent superpositions (coherences) between the para and ortho states, which evolve with the tunnelling frequency.

Thus we find that the connection to the higher level causes a shift of the coherent tunnelling frequency to

$$\upsilon_{ta}{}' = \upsilon_{ta} + \frac{k_{ab}k_{ba}}{k_{ba}^2+\upsilon_{tb}^2}\,\upsilon_{tb} \tag{21.40}$$

and in addition a damping of the singlet triplet coherences by a relaxation rate

$$r_{12} = \left(\frac{k_{ab}\upsilon_{tb}^2}{k_{ba}^2+\upsilon_{tb}^2}\right) \tag{21.41}$$

For the interpretation of this relaxation rate it is useful to transform the Liouville operator in the localized base. The transformation matrix in Hilbert space is

$$\hat{S} = \frac{1}{\sqrt{2}}\begin{pmatrix} 1 & 1 \\ 1 & -1 \end{pmatrix} \tag{21.42}$$

and the corresponding transformation super operator in Liouville space is from the transformation matrix as [82]

$$\hat{\hat{S}} = \hat{S}\otimes\hat{S} = \frac{1}{2}\begin{pmatrix} 1 & 1 & 1 & 1 \\ 1 & -1 & 1 & -1 \\ 1 & 1 & -1 & -1 \\ 1 & -1 & -1 & 1 \end{pmatrix} \tag{21.43}$$

where we have used the fact that $\hat{S}$ is a real matrix. Employing this operator, the equation in the localized space becomes

WILEY-VCH
Schowen
1. UK
N. Denzau

Kühn & Weyh Satz und Medien
Freiburg
l:/Vch/Schowen/3b2/c21.3d
19. 7. 2006

$$\begin{aligned}\frac{\mathrm{d}}{\mathrm{d}t}\hat{\hat{S}}\begin{pmatrix}\rho_{a1}\\ \rho_{a2}\\ \rho_{a3}\\ \rho_{a4}\end{pmatrix} &= \hat{\hat{S}}\begin{pmatrix}0 & 0 & 0 & 0\\ 0 & -r_{12}-\mathrm{i}\upsilon_{ta}{}' & 0 & 0\\ 0 & 0 & -r_{12}+\mathrm{i}\upsilon_{ta}{}' & 0\\ 0 & 0 & 0 & 0\end{pmatrix}\hat{\hat{S}}^{-1}\hat{\hat{S}}\begin{pmatrix}\rho_{a1}\\ \rho_{a2}\\ \rho_{a3}\\ \rho_{a4}\end{pmatrix}\\ &= \left[\begin{pmatrix}-\frac{1}{2}r_{12} & 0 & 0 & \frac{1}{2}r_{12}\\ 0 & -\frac{1}{2}r_{12} & \frac{1}{2}r_{12} & 0\\ 0 & \frac{1}{2}r_{12} & -\frac{1}{2}r_{12} & 0\\ \frac{1}{2}r_{12} & 0 & 0 & -\frac{1}{2}r_{12}\end{pmatrix}\right.\\ &\quad \left.+\,\mathrm{i}\begin{pmatrix}0 & \frac{1}{2}\upsilon_{ta}{}' & -\frac{1}{2}\upsilon_{ta}{}' & 0\\ \frac{1}{2}\upsilon_{ta}{}' & 0 & 0 & -\frac{1}{2}\upsilon_{ta}{}'\\ -\frac{1}{2}\upsilon_{ta}{}' & 0 & 0 & \frac{1}{2}\upsilon_{ta}{}'\\ 0 & -\frac{1}{2}\upsilon_{ta}{}' & \frac{1}{2}\upsilon_{ta}{}' & 0\end{pmatrix}\right]\hat{\hat{S}}\begin{pmatrix}\rho_{a1}\\ \rho_{a2}\\ \rho_{a3}\\ \rho_{a4}\end{pmatrix}\end{aligned} \tag{21.44}$$

The first term has a very simple physical interpretation. It corresponds to an incoherent exchange of the localized particles with an exchange rate

$$k_{12} = \frac{1}{2}r_{12} = \frac{1}{2}\left(\frac{k_{ab}\upsilon_{tb}^2}{k_{ba}^2+\upsilon_{tb}^2}\right) \tag{21.45}$$

between the localized states, i.e. an incoherent tunneling of the protons or deuterons from the left side to the right side of the potential.

$$\hat{\hat{K}} = \begin{pmatrix}-k_{12} & 0 & 0 & k_{12}\\ 0 & -k_{12} & k_{12} & 0\\ 0 & k_{12} & -k_{12} & 0\\ k_{12} & 0 & 0 & -k_{12}\end{pmatrix} \tag{21.46}$$

In the case of $v_{tb} >> k_{ba}$ this equation simplifies to

$$k_{12} = \frac{1}{2}k_{ab} \tag{21.47}$$

This result has a very intuitive explanation, which is sketched in Fig. 23.3. The rate k_{ab} is the transport rate from the ground state to the excited state. k_{ab} is much smaller then the decay rate k_{ba}. As soon as a molecule is excited to the higher state, the tunneling gets so fast that there is equal probability to find the particle on both sides, when it decays back into the ground state.

Thus, depending on the size of the barrier height, the two hydrons will exhibit strong differences in their dynamic behavior. For a low barrier height, a large tunnel frequency is observed. The dihydrogen pair will be at least partially delocalized and acts more or less like a one-dimensional free quantum mechanical rotor, similar to p-H_2 and o-H_2, allowing coherent (i.e. strictly periodic) exchange processes of the individual hydrons with the tunnel frequency ν_t. For high potential barriers the tunnel splitting goes to zero, no coherent exchange processes take place, each hydron is located in a single potential minimum and the dihydrogen pair is fixed.

WILEY-VCH
Schowen
1. UK
N. Denzau

Kühn & Weyh Satz und Medien
Freiburg
l:/Vch/Schowen/3b2/c21.3d
19. 7. 2006

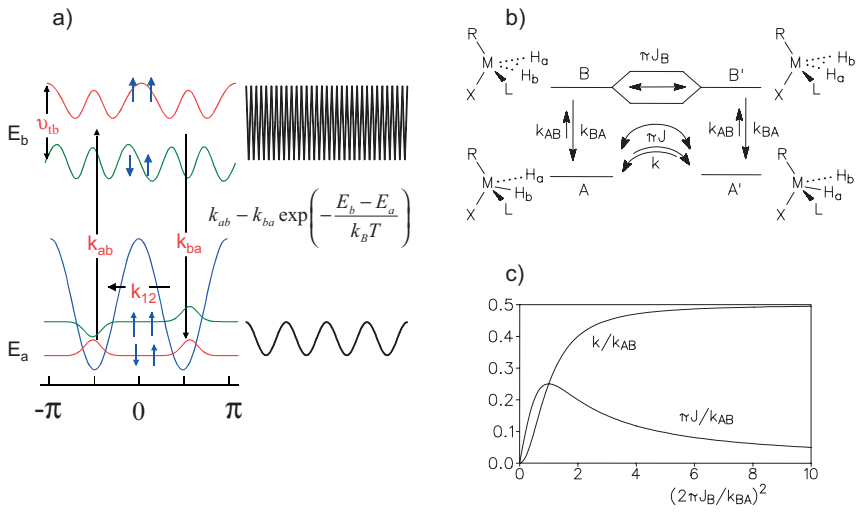

Figure 21.3 Sketch of the transition from coherent to incoherent tunneling: (a) Quantitative four-level model [86]; (b) corresponding chemisty of coherent and incoherent dihydrogen exchange [19]; (c) dependence of coherent and incoherent rates [19].

In this situation, for an exchange of the two hydrons a coupling to external degrees of freedom is necessary. In this scenario the exchange of the two hydrogen atoms is describable as a thermally activated rate process. Compared to the previous coherent exchange, the thermally activated rate process corresponds to an incoherent exchange of the two hydrons, which leads to an exponentially decaying curve for the probability of finding one hydron on its initial position.

21.2.2
Incoherent Tunneling and the Bell Model

As we have seen in the previous section there is a transition from coherent to incoherent tunneling, caused by the coupling to external bath degrees of freedom. This second type of tunnel process is the classical forbidden penetration of a barrier (Fig. 21.4), as for example in the Gamow model of ■-decay [87, 88] or the field emission of electrons of Condon [89, 90]. The probability of penetrating the barrier depends on the energy of the incident particle and the width, shape and height of the potential barrier. For most potentials only approximate solutions, as for example the well-known Wenzel [91], Kramers [92], Brilloiun [93] WKB approximation (see for example the textbook [80]), or numerical calculations of the transition probability are possible. Analytically solvable exceptions include rectangular potential steps and parabolic potentials. While the former give only very crude approximations of a real world system, the latter gives reasonably good results, when compared to experimentally determined rate constants.

WILEY-VCH
Schowen
1. UK
N. Denzau

Kühn & Weyh Satz und Medien
Freiburg
l:/Vch/Schowen/3b2/c21.3d
19. 7. 2006

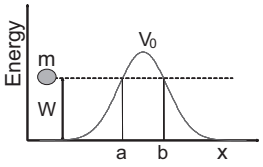

Figure 21.4 Tunneling through an energy barrier: While the particle m with energy $W < V_0$ is classically reflected at a, quantum mechanics allows a tunneling through the barrier from **a** to **b**.

As soon as bound states are considered there are only discrete energy levels. Nevertheless it was shown by Bell [77] that it is possible to employ approximately a continuum of energy levels for the calculations of the tunnel rates, which is adequate for the description of many experimental systems. In the simplest form (see Fig. 21.5) of the Bell model, the potential barrier is an inverted parabola. This allows the use of the known solution of the quantum mechanical harmonic oscillator for the calculation of the transition probability through the barrier. The corresponding Schrödinger equation is

$$\left[\frac{\mathrm{d}^2}{\mathrm{d}x^2} + \frac{2m}{\hbar^2}\left(E - \frac{1}{2}m\omega_0^2 x^2\right)\right]|\Psi\rangle = 0 \tag{21.48}$$

The ground state energy level is

$$E_0 = \frac{1}{2}\hbar\omega_0 =: \frac{1}{2}m\omega_0^2 a^2 \tag{21.49}$$

Here $2a$ is the width of the potential barrier at the ground state. Solving for $\nu_0 = \omega_0/2$ expresses the oscillation frequency via the ground state energy E_0 and the width of the potential at E_0:

$$\nu_0 = \frac{1}{\pi a}\sqrt{\frac{E_0}{2m}} \tag{21.50}$$

If the oscillator potential is inverted as shown in Fig. 21.5(b)

$$\left[\frac{\mathrm{d}^2}{\mathrm{d}x^2} + \frac{2m}{\hbar^2}\left(E + \frac{1}{2}m\omega_0^2 x^2\right)\right]|\Psi\rangle = 0 \tag{21.51}$$

the previous solution can be reused by introducing the imaginary tunnel frequency

$$\nu_\mathrm{t} = \frac{1}{\pi a}\sqrt{\frac{E_0}{2m}} \tag{21.52}$$

From this the probability for transition through the barrier

$$G(W) = \left[1 + \exp\left(\frac{V_0 - W}{h\nu_\mathrm{t}}\right)\right]^{-1} \tag{21.53}$$

WILEY-VCH
Schowen
1. UK
N. Denzau
Kühn & Weyh Satz und Medien
Freiburg
l:/Vch/Schowen/3b2/c21.3d
19. 7. 2006

is calculated. In typical chemical reactions large numbers of particles N_0 are involved. They are modeled as a stream $J = dN/dt$ of particles hitting the barrier. In thermal equilibrium the number of particles in energy interval $[W, W + dW]$ is given by the Boltzmann distribution

$$\begin{aligned} dN &= N_0 \cdot p(W)dW \\ &= N_0 \cdot \frac{1}{kT}\exp\left(-\frac{W}{kT}\right)dW \end{aligned} \tag{21.54}$$

If $T(W)$ is the transition probability at energy W, the number of particles per second, which pass the energy barrier is

$$J = J_0 \int_0^\infty p(W)T(W)dW \tag{21.55}$$

Quantum mechanically the transition rate J_{QM} of the Bell model is calculated by inserting Eq. (21.53) into Eq. (21.55).

$$\begin{aligned} J_{QM} &= \frac{J_0}{kT}\int_0^\infty \exp\left(-\frac{W}{kT}\right)G(W)dW \\ &= \frac{J_0}{kT}\int_0^\infty \exp\left(-\frac{W}{kT}\right)\left[1+\exp\left(\frac{V_0 - W}{h\nu_t}\right)\right]^{-1}dW \end{aligned} \tag{21.56}$$

Comparing this to the classically allowed rate from Arrhenius law

$$J_c = J_0\exp\left(-\frac{V_0}{kT}\right) \tag{21.57}$$

one can define the tunnel correction:

$$Q_t = \frac{J_{QM}}{J_c} = \frac{\exp(V_0/kT)}{kT}\int_0^\infty \exp\left(-\frac{W}{kT}\right)G(W)dW \tag{21.58}$$

For the numerical evaluation, Eq. (21.58) can be approximated by replacing the integration with a discrete sum over a set of energy levels. The result of such an evaluation is displayed in Fig. 21.5(d), which compares the classical Arrhenius rate with the quantum mechanical rates calculated from Eq. (21.56).

21.3
Symmetry Effects on NMR Lineshapes of Hydration Reactions

The symmetry effects associated with the Pauli principle provide an interesting diagnostic tool for the study of hydration and hydrogen transfer reactions. Employing spin-polarized parahydrogen (p-H_2) gas in these reactions, a very

WILEY-VCH
Schowen
1. UK
N. Denzau

Kühn & Weyh Satz und Medien
Freiburg
l:/Vch/Schowen/3b2/c21.3d
19. 7. 2006

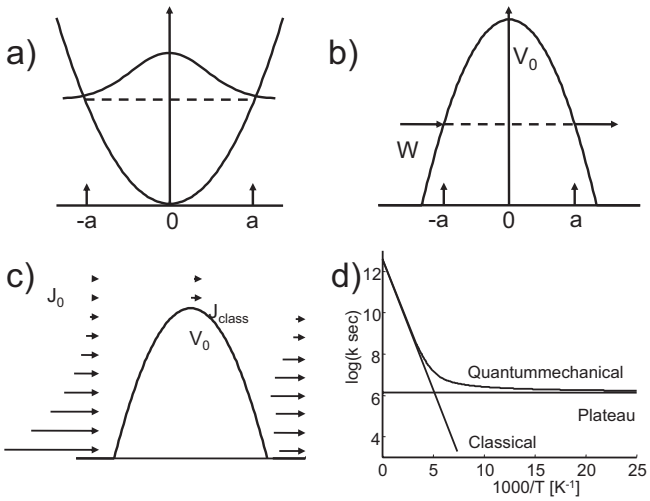

Figure 21.5 The Bell tunnel model: (a) Quantum mechanical harmonic oscillator with its ground state wavefunctions. (b) Inverted harmonic oscillator potential. (c) A stream of particles with a Boltzmann distribution of energies hits the barrier. Classical only those particles with $W > V_0$ can pass the barrier. Quantum mechanically particles with $W < V_0$ may also pass the barrier. (d) Comparison of classical Arrhenius rate and quantum mechanical corrected rate. While classically the rate goes to zero for $T \rightarrow 0$, quantum mechanically a finite plateau is approached (adapted after Bell [77]).

strong signal enhancement and thus selective spectroscopy of the reaction side is possible, as originally proposed by Bowers and Weitekamp [51, 56].

The origins of symmetry induced nuclear polarization can be summarized as follows: as mentioned above molecular dihydrogen is composed of two species, para-H_2, which is characterized by the product of a symmetric rotational wavefunction and an antisymmetric nuclear spin wave function and ortho-H_2, which is characterized by an antisymmetric rotational and one of the symmetric nuclear spin wavefunctions. In thermal equilibrium at room temperature each of the three ortho-states and the single para-state have practically all equal probability. In contrast, at temperatures below liquid nitrogen mainly the energetically lower para-state is populated. Therefore, an enrichment of the para-state and even the separation of the two species can be easily achieved at low temperatures as their interconversion is a rather slow process. Pure para-H_2 is stable even in liquid solutions and para-H_2 enriched hydrogen can be stored and used subsequently for hydrogenation reactions [54].

The transformation of this molecular rotational order into nuclear spin order during the hydrogenation reaction leads to typical polarization patterns in the NMR spectra of the hydrogenation products. Depending on whether the experiment is performed inside or outside of a magnetic field (see Fig. 21.6), these types of experiments have been referred to under the acronyms PASADENA (Parahydrogen and Synthesis Allow Dramatically Enhanced Nuclear Alignment) or

WILEY-VCH
Schowen
1. UK
N. Denzau
Kühn & Weyh Satz und Medien
Freiburg
l:/Vch/Schowen/3b2/c21.3d
19. 7. 2006

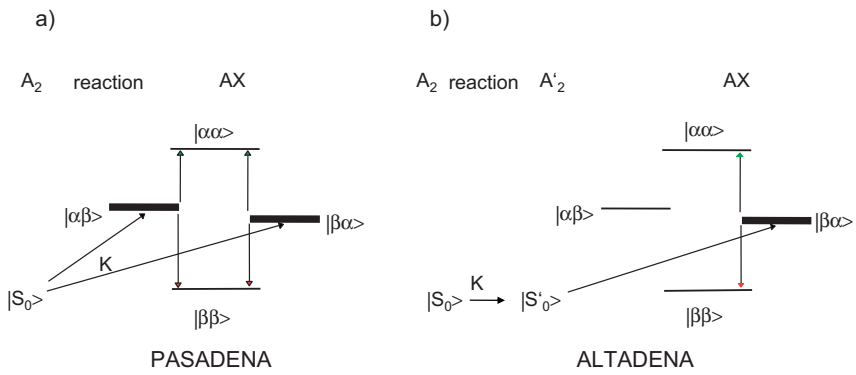

Figure 21.6 Schemes of simple PHIP experiments in an AX-spin system [56]. (a) Ideal PASADENA experiment. With the reaction rate *K* the population of the para-H_2 $|S_0>$ state is in a sudden change transferred to the $|\alpha\beta\rangle$ and $|\beta\alpha\rangle$ states, which are equally populated. (b) Ideal ALTADENA experiment. With the reaction rate *K* the population of the para-H_2 $|S_0>$ state is transferred to the $|S'_0>$ state of the final product. From there the population is adiabatically transferred to the $|\beta\alpha\rangle$ state of the final product, resulting in a selective population of this level (adapted from Bowers et al. [56]).

ALTADENA (Adiabatic Longitudinal Transport after Dissociation Engenders Net Alignment) [56]. All variants are nowadays known under the more generally acronym of PHIP (Parahydrogen Induced Polarization) [52]. The basic theory of the PHIP effect in an AX-spin system was given in the review paper of Bowers and Weitekamp [56].

In the original work only a simple AX-spin system with pure coherent exchange was considered. In practice, however, the situation will be a lot more complicated because there are several coherent and incoherent reaction pathways in the course of a catalyzed hydrogenation reaction, as depicted in Fig. 21.7.

To analyze these situations we first study analytically the PHIP effect for a general two spin system and then the effect of incoherent exchange on the PHIP line shape.

21.3.1
Analytical Solution for the Lineshape of PHIP Spectra Without Exchange

In the case of a simple reaction from the para-H_2 state to the product state it is possible to derive analytical solution of the lineshape of PHIP spectra [65]. In the following an alternative derivation of the lineshape is given. For simplicity the reaction is assumed as a one-way reaction, i.e. no back reaction (k_{ba}=0, *a*, *b* denote the two different sites).

For the para-H_2 state, the Hamiltonian is given as a pure A_2 spin system.

$$\hat{H}_a = J_a \hat{\vec{I}}_a \hat{\vec{S}}_a \tag{21.59}$$

WILEY-VCH
Schowen
1. UK
N. Denzau

Kühn & Weyh Satz und Medien
Freiburg
l:/Vch/Schowen/3b2/c21.3d
19. 7. 2006

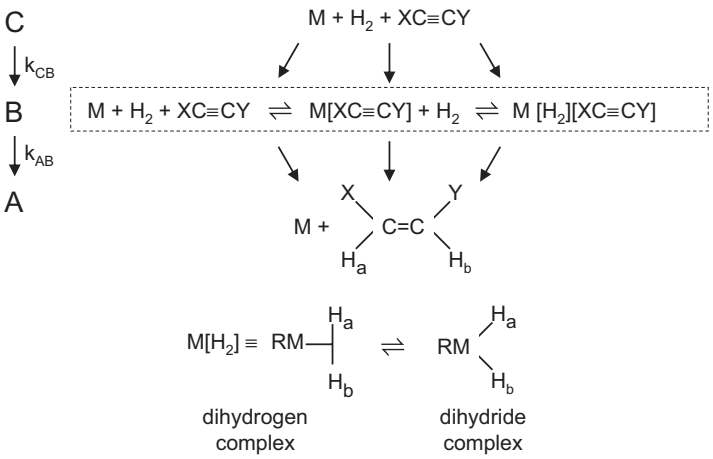

Figure 21.7 Possible pathways of the catalyzed hydrogenation reaction of an unsaturated organic substrate involving various transition metal dihydrogen and/or dihydride intermediates [62]. The initial free dihydrogen is labeled as site C, the intermediates containing the dihydrogen pair as B, and the product containing the dihydrogen pair as A.

For the end product of the reaction a general liquid Hamiltonian is assumed

$$\hat{H}_b = \nu_S \hat{S}_{zr} + \nu_I \hat{I}_{zr} + J_b \hat{\vec{I}}_b \hat{\vec{S}}_b, \tag{21.60}$$

which has the following matrix representation

$$\hat{H}_b = \begin{pmatrix} \frac{\nu_S+\nu_I}{2} + \frac{J_b}{4} & 0 & 0 & 0 \\ 0 & \frac{\nu_S-\nu_I}{2} + \frac{J_b}{4} & \frac{J_b}{2} & 0 \\ 0 & \frac{J_b}{2} & \frac{-\nu_S+\nu_I}{2} - \frac{J_b}{4} & 0 \\ 0 & 0 & 0 & \frac{-\nu_S-\nu_I}{2} + \frac{J_b}{4} \end{pmatrix} \tag{21.61}$$

The initial condition of the problem is that at the beginning all hydrogen atoms are in the singlet S_0 state of the para-H_2.

$$\begin{aligned} \rho(0) &= |S_0 >< S_0| \\ &= \frac{1}{2}|\alpha\beta - \beta\alpha >< \alpha\beta - \beta\alpha| \\ &= \frac{1}{4} - \hat{\vec{S}}\hat{\vec{I}} \\ &= \frac{1}{2}\begin{pmatrix} 0 & 0 & 0 & 0 \\ 0 & 1 & -1 & 0 \\ 0 & -1 & 1 & 0 \\ 0 & 0 & 0 & 0 \end{pmatrix} \end{aligned} \tag{21.62}$$

WILEY-VCH
Schowen
1. UK
N. Denzau

Kühn & Weyh Satz und Medien
Freiburg
l:/Vch/Schowen/3b2/c21.3d
19.7.2006

As a consequence of this the initial dynamics before any pulse is applied occurs only in the subspace spanned by the elements $\rho_a(22,23,32,33)$, $\rho_b(22,23,32,33)$ and the analysis of the dynamics can be restricted to this subspace. In the initial para-H_2 state, the equation of motion is:

$$\frac{\mathrm{d}}{\mathrm{d}t}\hat{\rho}_a = -\mathrm{i}\left[\hat{H}_a, \hat{\rho}_a\right] - k_{ab}\hat{\rho}_a \tag{21.63}$$

Since the Hamiltonian $\hat{H}_a$ commutes with $\hat{\rho}_a(0)$, no oscillations of the coherences are observed and the solution of the equation for $\rho_a(t)$ is simply given by an exponential decay

$$\hat{\rho}_a(t) = \exp(-k_{ab}t)\hat{\rho}_a(0) \tag{21.64}$$

In the next step the differential equation for $\rho_b(t)$ has to be solved:

$$\begin{aligned}\frac{\mathrm{d}}{\mathrm{d}t}\hat{\rho}_b &= -\mathrm{i}\left[\hat{H}_b, \hat{\rho}_b\right] + k_{ab}\hat{\rho}_a - \frac{1}{T_{2b}}\hat{\rho}_b \\ &= -\mathrm{i}\left[\hat{H}_b, \hat{\rho}_b\right] + k_{ab}\hat{\rho}_a(0)\exp(-k_{ab}t) - \frac{1}{T_{2b}}\hat{\rho}_b\end{aligned} \tag{21.65}$$

For the solution of this differential equation it is advantageous to transform the matrix equation of Hilbert space into a vector equation in Liouville space (E_b is the identity matrix of the four-dimensional subspace):

$$\hat{\hat{L}}_b = \hat{H}_b \otimes E_b - \hat{E}_b \otimes \hat{H}_b \tag{21.66}$$

The matrix representation of $\hat{\hat{L}}_b$ is

$$\hat{\hat{L}}_b = \begin{pmatrix} 0 & -\frac{J_b}{2} & \frac{J_b}{2} & 0 \\ -\frac{J_b}{2} & \Delta\nu & 0 & \frac{J_b}{2} \\ \frac{J_b}{2} & 0 & -\Delta\nu & -\frac{J_b}{2} \\ 0 & \frac{J_b}{2} & -\frac{J_b}{2} & 0 \end{pmatrix} \tag{21.67}$$

where we have introduced for abbreviation $\Delta\nu = \nu_{bS} - \nu_{bI}$. The inhomogeneous differential equation (21.65) becomes

$$\frac{\mathrm{d}}{\mathrm{d}t}\hat{\rho}_b = -2\mathrm{i}\pi\hat{\hat{L}}_b\hat{\rho}_b + k_{ab}\hat{\rho}_a(0)\exp(-k_{ab}t) - \frac{1}{T_{2b}}\hat{\rho}_b \tag{21.68}$$

The solution of Eq. (21.68) is

$$\begin{aligned}\hat{\rho}_b(t) = &\left(-2\mathrm{i}\pi\hat{\hat{L}}_b + k_{ab} - \frac{1}{T_{2b}}\right)^{-1} k_{ab} \\ &\times \left(\exp\left(\left(-2\mathrm{i}\pi\hat{\hat{L}}_b - \frac{1}{T_{2b}}\right)t\right) - \exp(-k_{ab}t)\right)\hat{\rho}_a(0)\end{aligned} \tag{21.69}$$

WILEY-VCH
Schowen
1. UK
N. Denzau

Kühn & Weyh Satz und Medien
Freiburg
l:/Vch/Schowen/3b2/c21.3d
19. 7. 2006

where the fact has been exploited that

$$\left[-2\pi i\hat{\hat{L}}_b - \frac{1}{T_{2b}} + k_{ab}, -2\pi i\hat{\hat{L}}_b - \frac{1}{T_{2b}}\right] = 0 \tag{21.70}$$

However, instead of directly evaluating Eq. (21.68) by Eq. (21.69) it is advantageous to combine the coherent evolution and the relaxation, i.e. the homogeneous part of Eq. (21.68) and transform the resulting matrix into a fictive spin –1/2 system, employing the normalized Pauli matrices as base vectors. The corresponding transformation is

$$\hat{\hat{S}}_1 = \frac{1}{2}\sqrt{2}\begin{pmatrix} 1 & 0 & 0 & 1 \\ 0 & 1 & 1 & 0 \\ 0 & 1 & -1 & 0 \\ 1 & 0 & 0 & -1 \end{pmatrix} \tag{21.71}$$

In this system, the matrix $\hat{\hat{L}}_b$becomes the block diagonal

$$\hat{\hat{L}}_b - \frac{1}{T_{2b}} = \begin{pmatrix} -\frac{1}{T_{2b}} & 0 & 0 & 0 \\ 0 & -\frac{1}{T_{2b}} & 2i\pi\Delta\upsilon & 0 \\ 0 & 2i\pi\Delta\upsilon & -\frac{1}{T_{2b}} & -2i\pi J_b \\ 0 & 0 & -2i\pi J_b & -\frac{1}{T_{2b}} \end{pmatrix} \tag{21.72}$$

It can be diagonalized in a second step by transforming with the matrix

$$\hat{\hat{S}}_2 = \begin{pmatrix} 1 & 0 & 0 & 0 \\ 0 & s & 0 & c \\ 0 & \frac{c}{\sqrt{2}} & \frac{1}{\sqrt{2}} & \frac{-s}{\sqrt{2}} \\ 0 & \frac{c}{\sqrt{2}} & \frac{-1}{\sqrt{2}} & \frac{-s}{\sqrt{2}} \end{pmatrix} \tag{21.73}$$

$$\text{with} \quad c = \frac{\Delta\nu}{\sqrt{(\Delta\nu^2 + J_b^2)}} \quad \text{and} \quad s = \frac{J_b}{\sqrt{(\Delta\nu^2 + J_b^2)}}$$

The resulting matrix of the homogeneous part is

$$\begin{pmatrix} -\frac{1}{T_{2b}} & 0 & 0 & 0 \\ 0 & -\frac{1}{T_{2b}} & 0 & 0 \\ 0 & 0 & -\frac{1}{T_{2b}} + 2i\pi\sqrt{(\Delta\upsilon^2 + J_b^2)} & 0 \\ 0 & 0 & 0 & -\frac{1}{T_{2b}} - 2i\pi\sqrt{(\Delta\upsilon^2 + J_b^2)} \end{pmatrix} = \varepsilon_\lambda \delta_{\lambda\mu} \tag{21.74}$$

Here the ε_λ denote the eigenvalues.

WILEY-VCH
Schowen
1. UK
N. Denzau

Kühn & Weyh Satz und Medien
Freiburg
l:/Vch/Schowen/3b2/c21.3d
19.7.2006

Applying the same transformation to the inhomogeneous part of Eq. (21.68) yields ($\hat{\sigma}$ denotes the density matrix in the transformed frame, i.e. $\hat{\sigma} = \hat{\hat{S}}_2\hat{\hat{S}}_1\hat{\rho}$):

$$\hat{\sigma}_a(t) = \hat{\hat{S}}_2\hat{\hat{S}}_1\rho_a(t) = \frac{1}{2}\begin{pmatrix}\sqrt{2}\\ \sqrt{2}\\ -c\\ -c\end{pmatrix} exp(-k_{ab}t) \tag{21.75}$$

With this the solution for the density matrix elements becomes (λ = 1.4, index of eigenvalue ε_k):

$$\sigma_{b\lambda}(t) = \frac{\sigma_{a\lambda}k_{ab}}{\varepsilon_\lambda - k_{ab}}(\exp(-k_{ab}t) - \exp(\varepsilon_\lambda t)) \tag{21.76}$$

Assuming that the oscillating matrix elements σ_{b3} and σ_{b4} disappear, a quasi-stationary limit of $\sigma_{b\lambda}$ can be calculated. If $T_2 \gg 1/k_{ab}$ and $T_2 \gg 1/(\Delta\nu^2+J_b^2)^{1/2}$ and $k_{ab} < (\Delta\nu^2+J_b^2)^{1/2}$ it follows for $t \to \infty$:

$$\begin{aligned}
\sigma_{b1}(\infty) &= \frac{1}{2}\sqrt{2}\\
\sigma_{b2}(\infty) &= -\frac{1}{2}\sqrt{2}\frac{J_b}{\sqrt{(J_b^2+\Delta\nu^2)}}\\
\sigma_{b3}(\infty) &= 0\\
\sigma_{b4}(\infty) &= 0
\end{aligned} \tag{21.77}$$

Transforming back into the original frame gives:

$$\begin{aligned}
\rho_{b1}(\infty) &= \frac{1}{2}\left(1 - \frac{\Delta\nu J_b}{(J_b^2+\Delta\nu^2)}\right)\\
\rho_{b2}(\infty) &= -\frac{1}{2}\frac{J_b^2}{(J_b^2+\Delta\nu^2)}\\
\rho_{b3}(\infty) &= -\frac{1}{2}\frac{J_b^2}{(J_b^2+\Delta\nu^2)}\\
\rho_{b4}(\infty) &= \frac{1}{2}\left(1 + \frac{\Delta\nu J_b}{(J_b^2+\Delta\nu^2)}\right)
\end{aligned} \tag{21.78}$$

The resulting spectral line can be calculated numerically from these elements of the density matrix. For the interpretation of the PHIP spectral line shape, the elements ρ_{b1} and ρ_{b4} are of particular interest, since they correspond to the level populations of the $|\alpha\beta\rangle$ and $|\beta\alpha\rangle$ states. Their dependence on J_b is shown in Fig. 21.8.

WILEY-VCH
Schowen
1. UK
N. Denzau

Kühn & Weyh Satz und Medien
Freiburg
l:/Vch/Schowen/3b2/c21.3d
19. 7. 2006

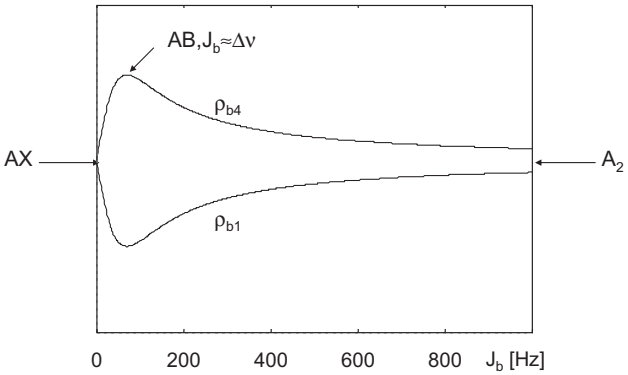

Figure 21.8 Calculation [86] of ρ_{b1} and ρ_{b4}, which are proportional to the populations of the $|\alpha\beta\rangle$ and $|\beta\alpha\rangle$ states in a PASADENA type PHIP experiment as a function of the coupling constant J_b. For a pure AX or A_2 system the populations are equal, while for an AB system deviations exist, which are strongest for $J_b \approx \Delta\nu$. Calculation with $\Delta\nu$ = 69 Hz.

21.3.2 Experimental Examples of PHIP Spectra

As mentioned above, PHIP is a versatile tool for the study of catalytic reactions. In the following three different experimental examples of this remarkable power, taken from recent work from the Bargon group followed from a theoretical example of reaction pathway sensitivity from our group are given. The experimental examples show a PHIP experiment performed under ALTADENA conditions, a PHIP experiment performed under PASADENA conditions and a PHIP experiment followed by a heteronuclear polarisation transfer from ^{1}H to ^{13}C.

21.3.2.1 PHIP under ALTADENA Conditions

The first example (see Fig. 21.9) shows a ^{1}H-PHIP spectrum of the hydration of perdeuterated styrene obtained under ALTADENA conditions, i.e. with hydration outside the NMR magnet taken from Ref. [94]. The spectrum of the hydration product ethyl-benzene exhibits the typical strong spin polarized signals at 1 ppm and 3 ppm. Between 5 ppm and 6 ppm there are additional spin polarized signals, which stem from a side reaction. In Ref. [94] it was shown that the ratio of hydration versus geminal exchange is controllable by addition of CO.

21.3.2.2 PHIP Studies of Stereoselective Reactions

PHIP allows also the PASADENA investigation of the stereoselectivity of a reaction. A typical example is given in Ref. [70], where the stereoselective hydrogenation of 3-hexyne-1-ol under the influence of the cationic ruthenium complex [Cp*Ru(η^4-

WILEY-VCH
Schowen
1. UK
N. Denzau

Kühn & Weyh Satz und Medien
Freiburg
l:/Vch/Schowen/3b2/c21.3d
19. 7. 2006

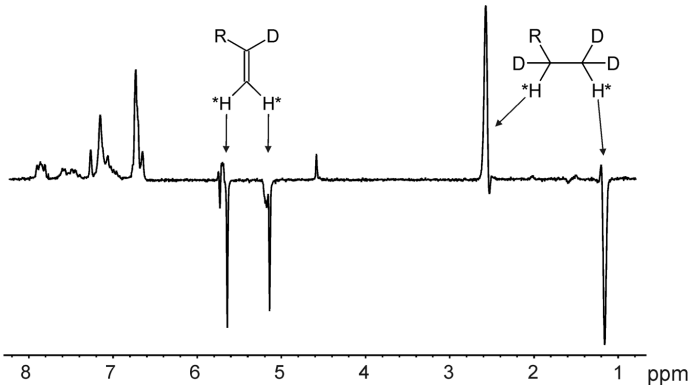

Figure 21.9 ^{1}H *in situ* PHIP NMR spectrum of the hydrogenation of styrene-d_8 using $H_2Ru(PPh_3)_4$ as catalyst measured under ALTADENA conditions (adapted from Ref. [94]).

$CH_3CH{=}CHCH{=}CHCOOH)][CF_3SO_3]$ is shown in a ^{1}H-PHIP experiment (see Fig. 21.10). The spectrum reveals the characteristic PHIP polarization pattern of adsorptive and emissive lines. This polarization pattern proves the pair-wise transfer of the para-hydrogen to the substrate. The observed anti-phase coupling constant of 15.5 Hz is a typical value for an olefinic trans coupling constant and identifies the formation of the corresponding (*E*)-alkene by trans-hydrogenation of the substrate.

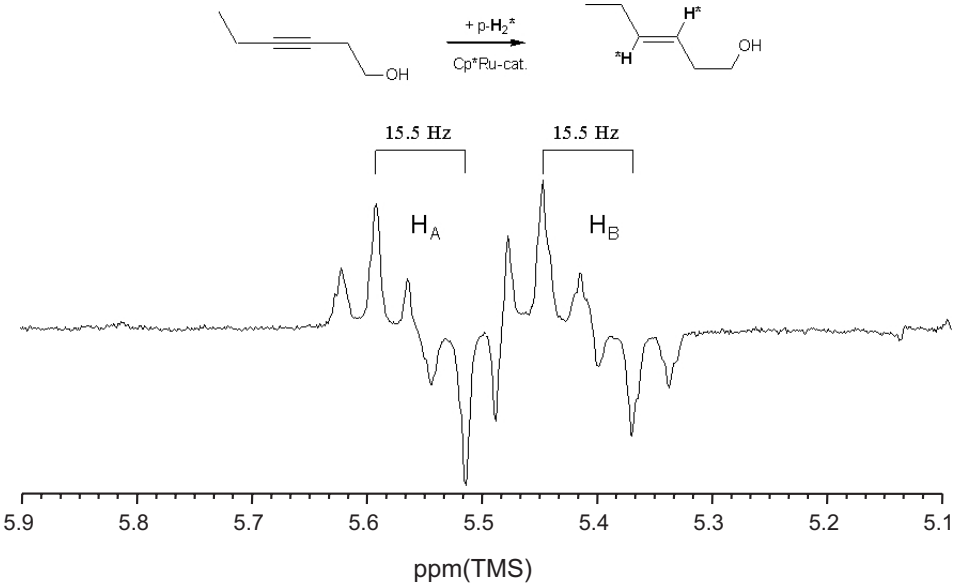

Figure 21.10 Olefinic region of a 200 MHz ^{1}H PHIP spectrum recorded during the hydrogenation of 3-hexyne-1-ol using Cp*Ru catalyst (adapted from Ref. [70]).

WILEY-VCH
Schowen
1. UK
N. Denzau

Kühn & Weyh Satz und Medien
Freiburg
l:/Vch/Schowen/3b2/c21.3d
19. 7. 2006

21.3.2.3 ^{13}C-PHIP-NMR

The last experimental example shows that PHIP is also a powerful starting point for sensitivity enhancement of NMR spectroscopy of hetero nuclei in catalytic reactions.

The homogeneously catalyzed hydrogenation of an unsaturated substrate with para-hydrogen leads not only to strong signal enhancements in ^{1}H NMR spectra, but can also give rise to strong heteronuclear polarization, in particular in ALTADENA type experiments where the hydrogenation is carried out in low magnetic fields. As a typical example taken from Ref. [74], the polarization transfer from protons to ^{13}C nuclei during the hydrogenation of 3,3-dimethylbut-1-yne with para-hydrogen and $[Rh(cod)(dppb)]^{+}$ as catalyst is shown in Fig. 21.11. In the single shot ^{13}C-NMR spectrum recorded *in situ* all ^{13}C resonances can be observed with good to excellent signal-to-noise ratios. The enhanced SNR is due to the PHIP effect resulting from a transfer of the initial proton polarization of the parahydrogen to the carbon atoms.

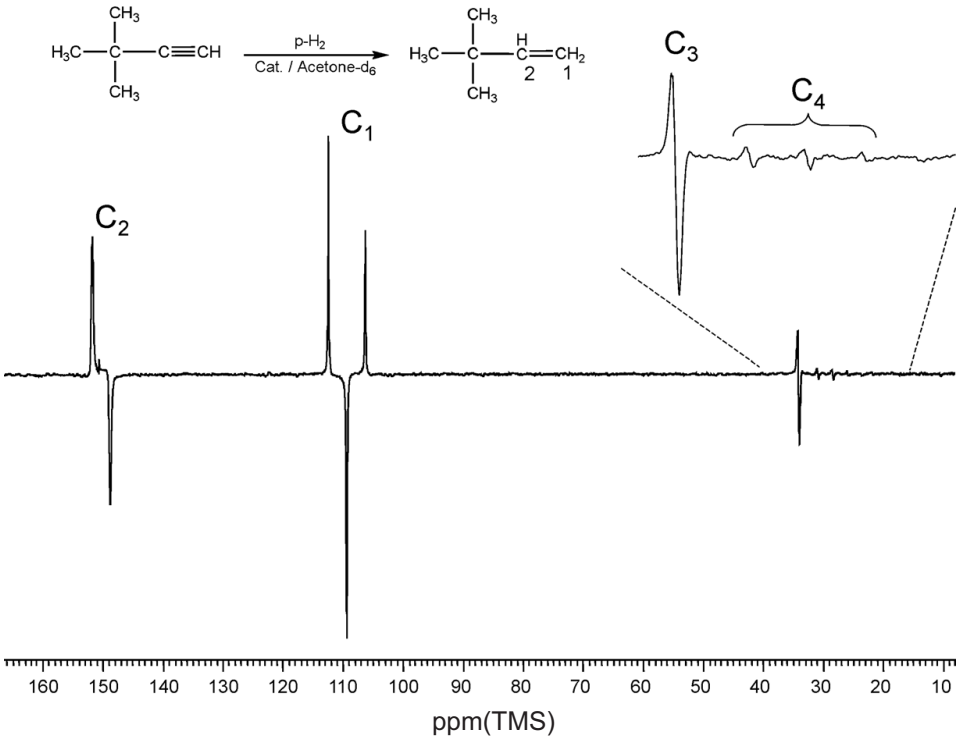

Figure 21.11 ^{13}C *in situ* PHIP spectrum after hydrogenation with para-hydrogen and polarisation transfer from protons to carbons. Note the extremely high signal/noise ratio in the single shot spectrum, which is a measure for the strong signal enhancement obtained by PHIP (adapted from Ref. [74]).

WILEY-VCH
Schowen
1. UK
N. Denzau
Kühn & Weyh Satz und Medien
Freiburg
l:/Vch/Schowen/3b2/c21.3d
19. 7. 2006

Due to the ALTADENA procedure, nuclear polarization is transferred to all magnetically active nuclei, since all resonance frequencies are virtually the same for all nuclei at the very low magnetic field of the Earth. The corresponding spin systems are of a high order, i.e. the difference in the resonance frequencies between the carbons (^{13}C) and the protons is small, compared with their coupling constants. This is an essential prerequisite for an efficient polarization transfer from protons to a large number of carbons.

21.3.3
Effects of Chemical Exchange on the Lineshape of PHIP Spectra

Equations (21.78) allow the calculation of PHIP spectra in the case of non-exchanging hydrogen atoms, i.e. for $k_{12} = 0$. If $k_{12} > 0$, however, the lineshape of the PHIP spectra does depend on the chemical exchange. Interestingly this allows one to extract information about reaction intermediates, which are not directly visible in the NMR spectra [62] owing to their short lifetime or low concentration.

Employing the quantum mechanical density matrix formalism it is possible to take into account the whole reaction pathway of Fig. 21.12 where both coherent and incoherent reaction pathways are present in the case of a PHIP experiment and convert the PHIP experiment into a diagnostic tool for all stages of a hydrogenation reaction. Such an analysis was performed in Ref. [62]. In these calculations the initial condition was that at the start of the reaction all molecules are in the p-H_2 state of site C, i.e., a pure singlet spin state, represented as a circle in Fig. 21.12, which shows the different possible reaction pathways. Moreover, all intermolecular exchange reactions were treated as one-sided reactions, i.e. the rates of the back reactions were set to zero.

Two different scenarios are analyzed, namely where the reaction goes as a two-step process, as depicted in Fig. 21.12(a) or where the reaction goes as a three-step process (Fig. 21.12(b)).

Accordingly in Fig. 21.12(a) only two sites r = C or A are included. For simplicity, only the forward reactions are shown, but in the formalism the backward reactions are also included. In both sites C and A the possibility for incoherent exchange of the two hydrogen atoms H_a and H_b, characterized by the rate constants k_{CC} and k_{AA} is included. In addition, the parameter p_{CA} is introduced, which describes the regio-selectivity of the reaction between C and A. It represents the probability of permutation of the two hydrogen atoms during the transfer from C to A and A to C, respectively. The step is completely regio-specific if $p_{CA} = 0$ or 1 and completely non-selective when $p_{CA} = 0.5$ and partially regio-selective for other values of p_{CA}. In the latter two cases the reaction would lead to isotope scrambling if the reaction is performed with an HD pair as substrate. It is found that this regio-selectivity requires that the two protons are labeled prior to the reaction by different Larmor frequencies, otherwise it does not affect the results, as is the case if C corresponds to free dihydrogen; however, the regio-selectivity is important when an additional intermediate B is included in the more general case of Fig. 21.12(b) in which the two former para-H_2 protons are chemically different.

WILEY-VCH
Schowen
1. UK
N. Denzau

Kühn & Weyh Satz und Medien
Freiburg
l:/Vch/Schowen/3b2/c21.3d
19. 7. 2006

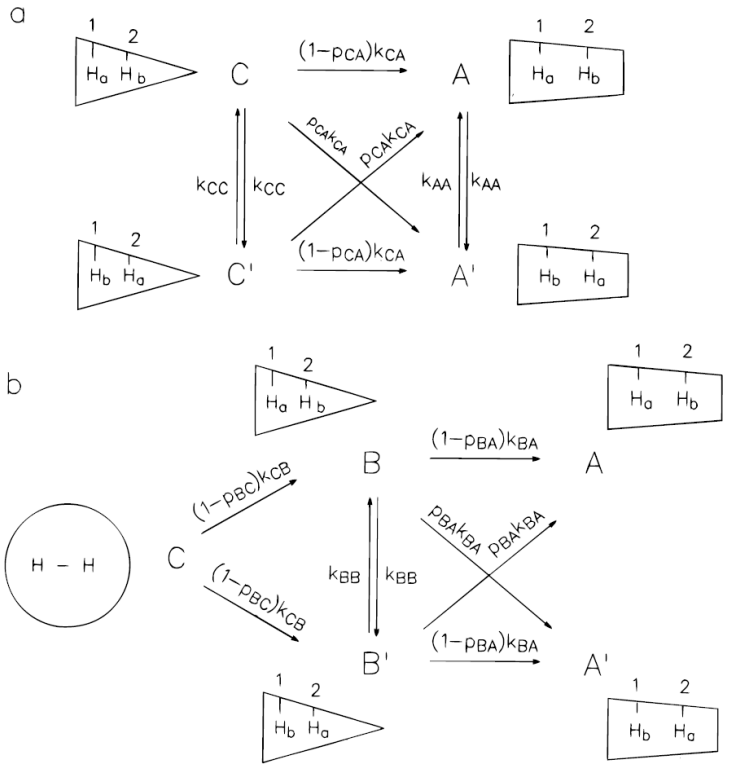

Figure 21.12 Formal two-site (a) and three-site (b) reaction models of a single (a) and two-step (b) hydrogenation reaction [62]. *prs* = *psr*, *r*, *s* = A to C represents the parameter characterizing the probability of permutation of the two hydrogen atoms during the interconversion between *r* and *s*. The step is called regio-specific if *prs* = 0 or 1, non-regio-specific if *prs* = 0.5, and otherwise it is called regio-selective.

In the following, the effects of these exchange processes and isotope scrambling on the level populations and line shapes of the PHIP experiment are shown. Details of the numerical calculations are found in the original paper [62].

Figure 21.13 shows the dependence of the density matrix elements ρ_{22} and ρ_{33} on the mutual exchange rate k_{AA} in a two-step experiment. It is evident that the mutual exchange removes the differences in the populations of the two levels $|\alpha\beta\rangle$ and $|\beta a\rangle$ and thus will change the appearance of the PHIP spectra. Figure 21.14 displays this effect of an incoherent mutual exchange of the two protons in the product site A, characterized by the rate constant k_{AA} on the PHIP spectra. Without mutual exchange there are strong differences in the line intensity pattern and the outer lines are higher than the inner ones. In the case of mutual exchange however, the intensity pattern of the normal NMR spectrum is obtained. These magnetization transfer effects are most pronounced in the case of the AB case where $J_A/\Delta\nu_A \approx 1$, (bottom spectrum). By contrast, AX-type spectra are practically

WILEY-VCH
Schowen
1. UK
N. Denzau

Kühn & Weyh Satz und Medien
Freiburg
l:/Vch/Schowen/3b2/c21.3d
19. 7. 2006

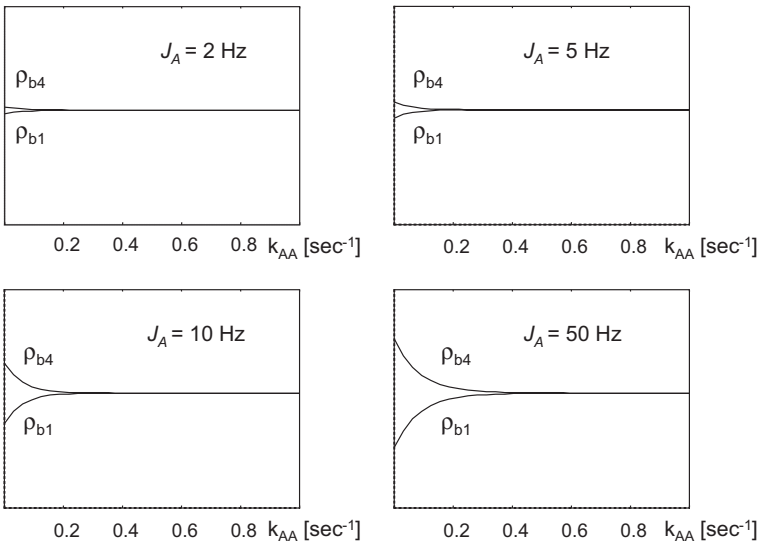

Figure 21.13 Calculation of ρ_{22} and ρ_{33} in a PASADENA type PHIP experiment as a function of the self exchange rate k_a for different spin systems [86]. In all cases the self-exchange leads to an averaging of the populations of ρ_{22} and ρ_{33}.

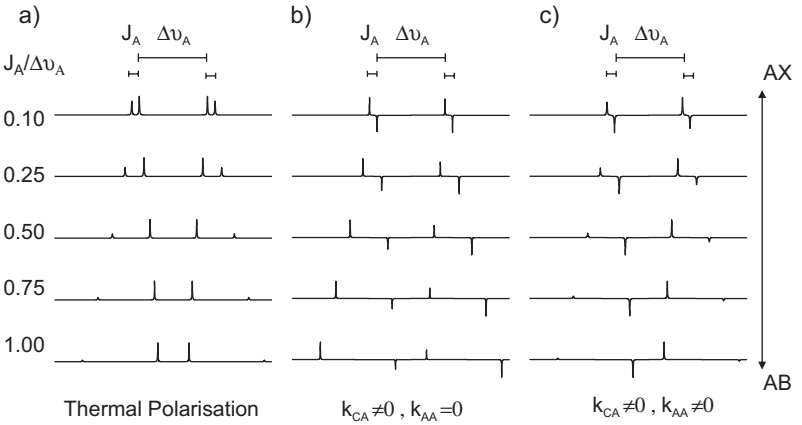

Figure 21.14 Calculated [62] NMR (a) and PHIP NMR (b,c) spectra of a two-proton spin system of compound A as a function of the ratio $J_A / \Delta\nu_A$, produced in a PASADENA experiment with (π/4) x pulses by the two-site reaction C → A (reaction time tr = 10 s; rate constant k_{CA} = 1 s^{-1}). (b) Without self-exchange. The ratios of the absolute outer and inner line intensities differ from those of the normal NMR spectra (not shown). (c) a self-exchange of the two protons during the reaction time tr is introduced with k_{AA} = 1 s^{-1} resulting in relative absolute PHIP-signal intensities corresponding to those of the normal NMR spectrum (a) (adapted from Ref. [62]).

WILEY-VCH
Schowen
1. UK
N. Denzau
Kühn & Weyh Satz und Medien
Freiburg
l:/Vch/Schowen/3b2/c21.3d
19. 7. 2006

not influenced by the exchange, neglecting the minor broadening effect of the lines which is not important for the present discussion.

Calculations of the PASADENA pattern for regio-selecitvities p_{AB} between 0 and 1 showed that the resulting density matrices and, therefore, the calculated PHIP spectra, are independent of this parameter. This is the expected result because in p-H2 the two protons are indistinguishable.

Figure 21.15 shows the dependence of the density matrix elements ρ_{b1} and ρ_{b4} on the mutual exchange rate k_{AA} in a three-step experiment. While the mutual exchange again removes the differences in the populations of the two levels $|\alpha\beta\rangle$ and$|\beta\alpha\rangle$, the strength of the effect now depends on the lifetime of the reaction intermediate B. If this lifetime is short compared to the inverse exchange rate, the density matrix elements are only weakly affected. If the life time is long enough, however, both levels get equally populated (Fig. 21.15(b)). Moreover the region-selectivity of the reaction now also strongly influences the population numbers (Fig. 21.15(c),(d)). Again these changes in the population numbers have a strong influence on the appearance of the PHIP spectra. Figure 21.16 shows the resulting PHIP signal patterns of A formed in the three-site-reaction PASADENA of Fig. 21.12(b). The four sets of spectra illustrate the influence of k_{BB} and of $J_B/\Delta\nu_B$. If B constitutes an AX spin system ($J_B/\Delta\nu_B$), the resulting spectra show no depen-

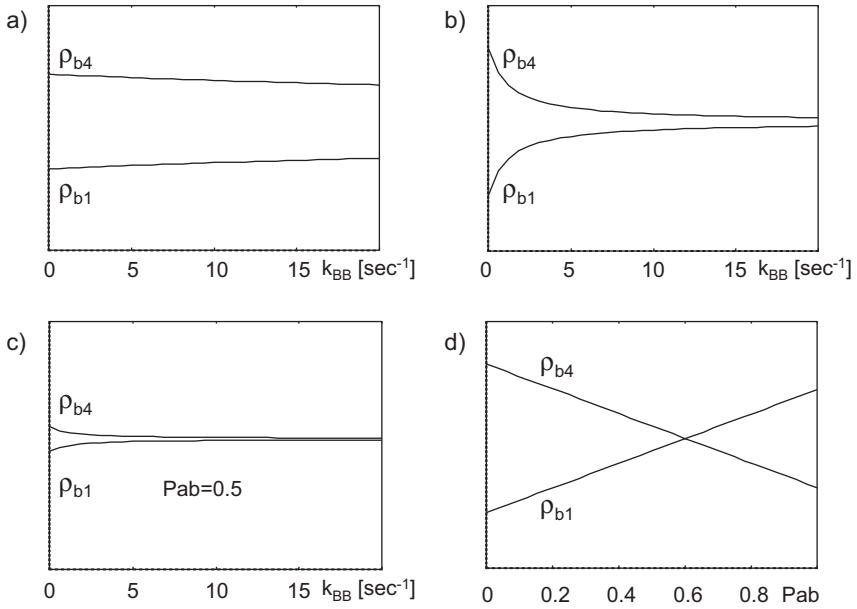

Figure 21.15 The calculation of ρ_{22} and ρ_{33} in a three-site PASADENA experiment as a function of the self-exchange rate k_{BB} for an AB system for different production and decay rates: (a) completely regio-specific, $K_{cb} = 1\ s^{-1}$ $K_{ba} = 1\ s^{-1}$; (b) completely region-specific, $K_{cb} = 1\ s^{-1}$ $K_{ba} = 100\ s^{-1}$; (c) completely non-regio-specific; (d) dependence on the region selectivity parameter [86].

WILEY-VCH
Schowen
1. UK
N. Denzau
Kühn & Weyh Satz und Medien
Freiburg
l:/Vch/Schowen/3b2/c21.3d
19. 7. 2006

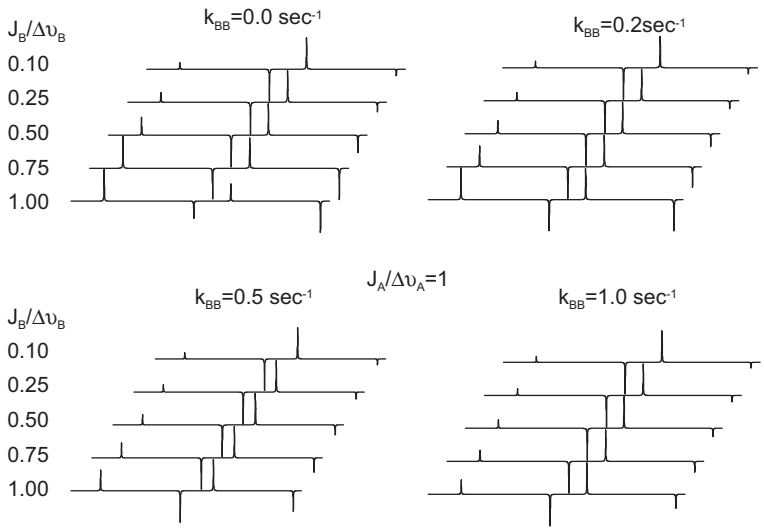

Figure 21.16 Calculated PHIP signal patterns (adapted from Ref. [62]) of a hydrogenation product A resulting in a PASADENA experiment in the presence of the three-site reaction C→B→A as a function of the ratio $J_B/\Delta\nu_B$. Note the differences in the line intensities (inner versus outer lines).

dence on k_{BB} and the ratio between the absolute intensities of the outer and the inner lines corresponds to the normal spectrum. However, if B constitutes an AB spin system, as expected in the case of substantial but not too large exchange couplings, large effects are observed and the ratio between the absolute intensities of the outer and the inner lines has changed. Thus, in principle, the incoherent dihydrogen exchange, the exchange and magnetic couplings, and the chemical shifts of the two protons in the intermediate B, all leave fingerprints which can be deciphered from the PHIP pattern of A.

In conclusion, the numerical simulations of the PHIP spectra show that the PHIP patterns do not only depend on the type of the experiment performed – e.g. ALTADENA in the absence and PASADENA in the presence of a magnetic field – but also on the properties of possible reaction intermediates where the reactants are bound to the employed transition metal catalyst. The important parameters of the intermediate are the chemical shifts and coupling constants of the former p-H_2 protons, especially their exchange couplings, as well as the rate of an incoherent dihydrogen exchange. In addition, the regio-selectivity of the hydrogenation step is a factor determining the PHIP-patterns, whereby the individuality of the former p-H_2 atoms arises from different chemical shifts in the intermediate.

In summary the calculations presented in Ref. [62] represent the missing theoretical link between the phenomena of incoherent and coherent dihydrogen exchange in transition metal hydrides and the PHIP effect. Moreover, PHIP is identified as a powerful and sensitive tool to study reaction pathway effects via analysis of the polarization patterns of the final hydrogenation products.

WILEY-VCH
Schowen
1. UK
N. Denzau

Kühn & Weyh Satz und Medien
Freiburg
l:/Vch/Schowen/3b2/c21.3d
19. 7. 2006

21.4
Symmetry Effects on NMR Lineshapes of Intramolecular Dihydrogen Exchange Reactions

Symmetry induced tunneling effects influence not only hydration reactions but also intermolecular hydrogen exchange reactions. In the case of a dihydrogen exchange the spatial Schrödinger equation (Eq. (21.5)) and its solutions (Eq. (21.11)) were discussed in a previous section. Since the eigenfunctions obey the Pauli principle they couple to spin functions in accordance with their symmetry and the spin of the hydrogen isotope (i.e. $^1/_2$ for ^{1}H, ^{3}H and 1 for ^{2}H) and the whole dynamics of the system can again be described purely in a spin Hilbert space.

The spin Hamiltonian of the system consists of three parts: The chemical shifts and/or quadrupolar interactions define the individual Hamiltonians of the spins $\hat{\vec{I}}_1$ and $\hat{\vec{I}}_2$ and the dipolar couplings and exchange interactions define the coupling Hamiltonian $\hat{H}_{1,2}\left(\hat{\vec{I}}_1, \hat{\vec{I}}_2\right)$. The mutual exchange of the two nuclei corresponds to a permutation of the two nuclei which exchange their individual chemical shifts and/or quadrupolar couplings with exchange rates $k_{12} = k_{21} = k$.

A relatively formal derivation in Ref. [11], which is based on the NMR lineshape analysis ideas of Alexander and Binsch [95, 96] shows that the whole dynamics is determined by the following Liouville von Neumann equation for the density matrix ρ_g:

$$\frac{\mathrm{d}}{\mathrm{d}t}|\rho_g) = -(\hat{\hat{W}}_A + \hat{\hat{K}})|\rho_g) \tag{21.79}$$

Here $\hat{\hat{W}}_A$ is the sum of the Liouville super operator $\hat{\hat{L}}_A$ and the relaxation super operator $\hat{\hat{R}}_A$.$\hat{\hat{K}}$ is the the self-exchange superoperator

$$\hat{\hat{K}} = -k(\hat{\hat{I}}_d - \hat{\hat{P}}_{12}) \tag{21.80}$$

which describes the exchange of the two nuclei in Liouville space. Its elements are the identity operator $\hat{\hat{I}}_d$ and the permutation superoperator $\hat{\hat{P}}_{12}$. The latter is calculated from the permutation operator in Hilbert space $\hat{P}\left(\hat{\vec{I}}_1, \hat{\vec{I}}_2\right)$ (Eq. (21.16)) via

$$\hat{\hat{P}} = \hat{P}\left(\hat{\vec{I}}_1, \hat{\vec{I}}_2\right) \otimes \hat{P}\left(\hat{\vec{I}}_1, \hat{\vec{I}}_2\right)^* \tag{21.81}$$

where $\hat{P}\left(\hat{\vec{I}}_1, \hat{\vec{I}}_2\right)^*$ denotes the complex conjugate of operator of $\hat{P}\left(\hat{\vec{I}}_1, \hat{\vec{I}}_2\right)$.

21.4.1
Experimental Examples

The energy differences between the tunnel levels and thus the tunnel frequency depend very strongly on the hindering potential $2V_0$ and vary between zero and

WILEY-VCH
Schowen
1. UK
N. Denzau
Kühn & Weyh Satz und Medien
Freiburg
l:/Vch/Schowen/3b2/c21.3d
19. 7. 2006

10^{12} Hz (see Fig. 21.2) i.e. over roughly twelve orders of magnitude. As a result of this extremely broad possible dynamic range, no single spectroscopic technique is able to cover the range of possible tunnel splitting. It follows that the experiment must be chosen according to the size of the expected tunnel frequency. While slow tunneling processes can be studied by ^{1}H liquid state NMR spectroscopy, intermediate processes are accessible by ^{2}H solid state NMR spectroscopy and relaxometry and fast processes are accessible by incoherent neutron scattering (INS). Fortunately the dynamic ranges of these techniques overlap partially. From this it follows that, at least in principle, a complete tunneling kinetics can be determined by combining some of these techniques.

In the following three experimental examples of such quantum mechanical exchange processes are discussed. The examples are taken from liquid state NMR spectroscopy, solid state NMR spectroscopy and INS.

21.4.1.1 Slow Tunneling Determined by ^{1}H Liquid State NMR Spectroscopy.

As discussed above in ^{1}H liquid state NMR a tunnel splitting, i.e. exchange coupling, and a conventional magnetic J-coupling have the same influence on the ^{1}H liquid state NMR spectra. This theoretical fact is nicely demonstrated in Fig. 21.17). It displays the superimposed experimental and calculated 1H liquid state NMR hydride signals of (C5Me5)RuH3(PCy3) (Cy = cyclohexyl) **1** dissolved in tetrahydrofuran-*d8* [19]. At low temperatures site 2 exhibits a triplet splitting characterized by a temperature dependent exchange coupling constant $J12 = J23$. A coupling constant $J24$ with the 31P nucleus in site 4 cannot be resolved. Sites 1 and 3 are equivalent and exhibit the expected doublet splitting with the nucleus in site 2, as $J12 = J23$. Furthermore, each line component is split by scalar coupling with the 31P nucleus in site 4 with $J14 = J34 = 32$ Hz. In contrast to $J14$, corresponding to a magnetic coupling, $J12$ represents an exchange coupling which increases strongly with temperature, as revealed by the typical AB2X signal pattern. Above 210 K, line broadening and coalescence occurs, eventually leading to a doublet with an average splitting of $J(^1H–^{31}P) = (J14 + J24 + J34)/3 = 22$ Hz. This splitting indicates that the classical exchange process observed is purely intramolecular. By lineshape analysis the exchange coupling constants $J12$ and the rate constants k_{HH} of the classical exchange are obtained.

21.4.1.2 Slow to Intermediate Tunneling Determined by ^{2}H Solid State NMR

Liquid state NMR experiments like above only allow the determination of slow coherent and incoherent tunnel rates, owing to the limited frequency range of the hydrogen chemical shifts. Faster tunneling processes can be studied by ^{2}H solid state NMR spectroscopy [11, 40].

Figure 21.18 compares experimental ^{2}H solid echo NMR spectra and the simulated ^{2}H FID-NMR spectra of the Ru-D_2 complex trans-[Ru(D_2)Cl(dppe)$_2$]PF_6 (Ru-D_2). At temperatures below 10 K the singularities of a satellite Pake pattern are visible as a splitting of the spectra at ±60 kHz. This satellite Pake pattern is the

WILEY-VCH
Schowen
1. UK
N. Denzau

Kühn & Weyh Satz und Medien
Freiburg
l:/Vch/Schowen/3b2/c21.3d
19. 7. 2006

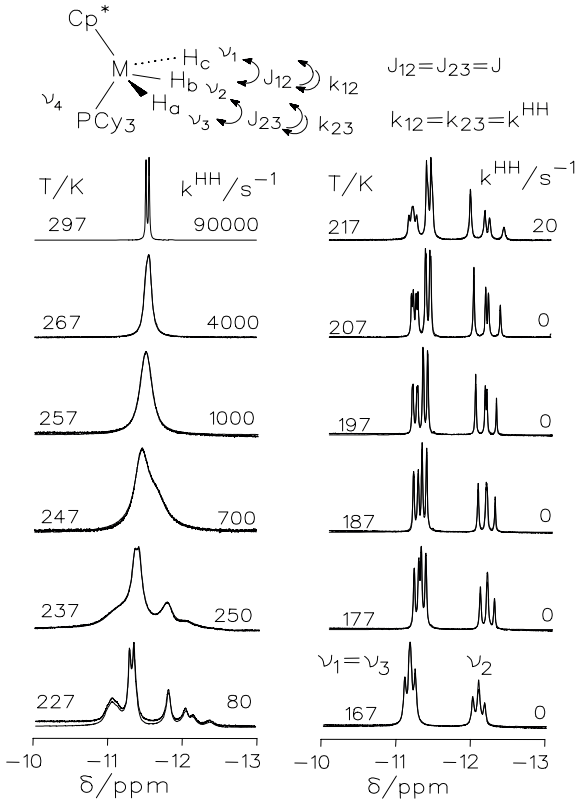

Figure 21.17 Superposed temperature dependent experimental and calculated 500 MHz 1H NMR hydride signals of $(C_5Me_5)RuH_3(PCy_3)$ (Cy = cyclohexyl) **1** dissolved in tetrahydrofuran-d_8 (adapted from Ref. [19]).

result of the coherent tunneling of the two η^2-bound deuterons in the complex. While the satellite transitions are fairly narrow at 5.4 K they start to smear out at higher temperatures. This smearing out is the effect of the incoherent tunneling which starts to dominate the dihydrogen dynamics and thus the spectral lineshape at higher temperatures.

At temperatures above 23 K the ^{2}H NMR line corresponds to a typical ^{2}H NMR quadrupolar Pake pattern with an asymmetry of $\eta = 0.2$. The satellite pattern has completely disappeared. The width of the line decreases slowly with increasing temperature, which is an indication of a weakening of the η^2-bond between the metal and dihydrogen.

Assuming the simple harmonic potential of Eq. (21.5) the height of the rotational barrier can be estimated. Using the value of R_{HH} = 1 Å, a rotational barrier of $2V_0 = 270$ meV (6.22 kcal mol^{-1}) is calculated.

WILEY-VCH
Schowen
1. UK
N. Denzau

Kühn & Weyh Satz und Medien
Freiburg
l:/Vch/Schowen/3b2/c21.3d
19. 7. 2006

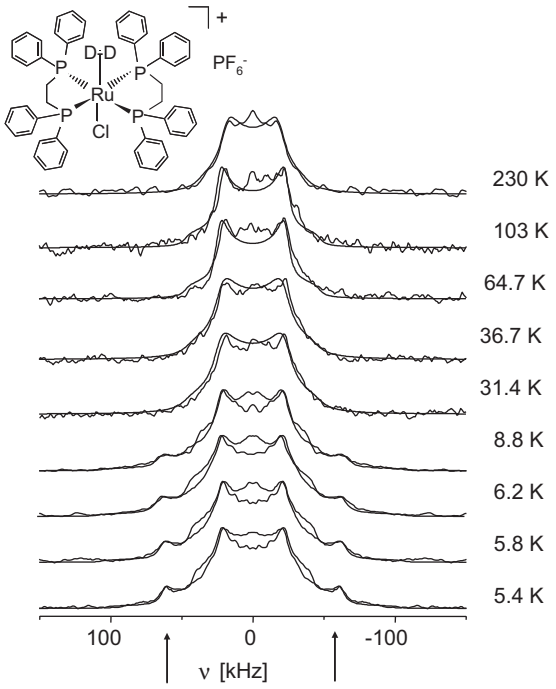

Figure 21.18 Experimental solid echo ^{2}H NMR spectra of the Ru-D_2 complex *trans*-[Ru(D_2)Cl(dppe)$_2$]PF_6 (Ru-D_2), measured in the temperature range 5.4 to 230 K. At temperatures below 8.8 K a splitting in the ^{2}H NMR lineshape is clearly visible (arrows). This splitting can be explained by a coherent tunneling of the two deuterons in the Ru-D_2 sample (simulation as ^{2}H FID-NMR experiment). The simulations were performed with $q_{zz} = 80\pm3$kHz (i.e. $q_{cc} = 107\pm4$kHz), $\eta = 0$ and a jump angle of $2\beta = 90°$ between the two tensor orientations (adapted from Ref. [40]).

21.4.1.3 **Intermediate to Fast Tunneling Determined by ^{2}H Solid State NMR**

Faster incoherent tunnelling processes can be studied by ^{2}H solid state NMR relaxometry [40, 41]. In these experiments the experimentally determined spin–lattice relaxation rates are converted into incoherent exchange rates. The latter are then evaluated, for example with the Bell tunnelling model described above.

As a first experimental example, Fig. 21.19 displays the result of the T_1 measurements on the same Ru-D_2 complex trans-[Ru(D_2)Cl(dppe)$_2$]PF_6 (Ru-D_2) as above. Due to the low sensitivity of the sample the spin–lattice relaxation rates were measured only at some selected temperatures. The lowest T_1 value (0.12±0.02 s) was found at 97 K. At low temperatures the T_1 data show strong deviations from simple Arrhenius behavior.

The exchange rates from the relaxation data are obtained for $K^{EFG} = 0.3\pi^2(60\text{ kHz})^2$ and the rate data from the spectra by lineshape analysis.

As a second experimental example, Fig. 21.20 presents the experimental results of the temperature dependence of the ^{2}H NMR spin–lattice relaxation time mea-

WILEY-VCH
Schowen
1. UK
N. Denzau

Kühn & Weyh Satz und Medien
Freiburg
l:/Vch/Schowen/3b2/c21.3d
19. 7. 2006

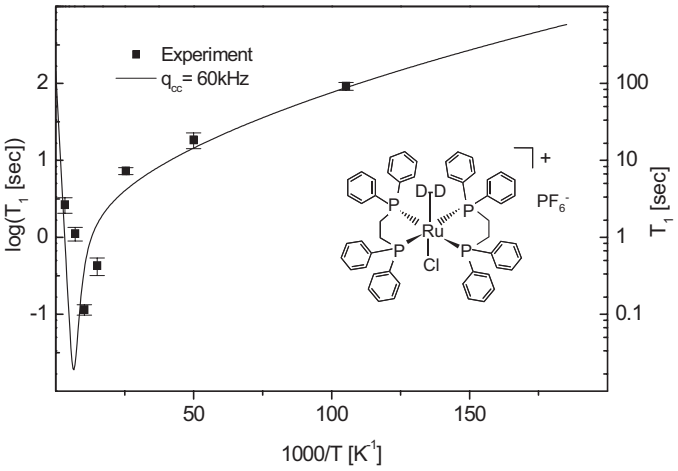

Figure 21.19 T_1relaxation data of the Ru-D_2 complex ((adapted from Ref. [40]). Experimental points from lineshape analysis and relaxation measurements. The solid line is calculated from the exchange rates calculated from the modified Bell model using the value of $K^{EFG} = 0.3\pi^2(60\ kHz)^2$.

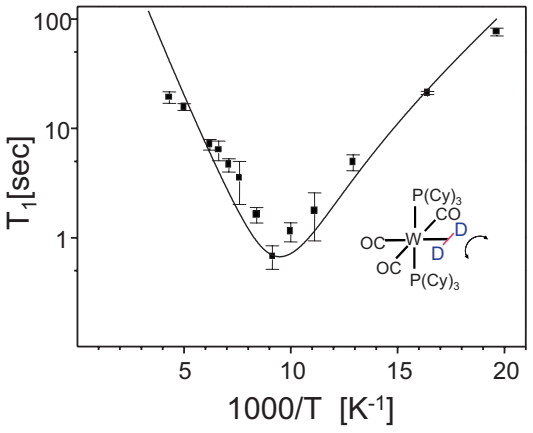

Figure 21.20 Experimental temperature dependence of the ^2H spin–lattice relaxation in the W-D_2 complex (adapted from Ref. [41]). The data exhibit deviations from Arrhenius behavior at low temperatures. The solid line is calculated from the exchange rates calculated from the Bell model.

surements on the W-D_2 complex W(PCy3)2(CO)3(η^2-D_2), also known as the Kubas complex, together with a calculation of the relaxation times. The T_1 measurements in the temperature regime from 50 to 230 K show a strong temperature dependence of T_1 with a sharp minimum close to 110 K. At the minimum a T_1

WILEY-VCH
Schowen
1. UK
N. Denzau
Kühn & Weyh Satz und Medien
Freiburg
l:/Vch/Schowen/3b2/c21.3d
19. 7. 2006

relaxation time of (0.68±0.15) s is found. It is evident that in the low temperature branch of the spin–lattice relaxation curve there are again deviations from a simple Arrhenius behavior, visible in a flattening of the curve.

21.4.1.4 **Fast Tunneling Determined by Incoherent Neutron Scattering**

Very fast coherent and incoherent tunneling processes can be studied by incoherent neutron scattering (INS). The basic mechanism of interpretation is closely related to the liquid state NMR experiment in the slow tunnel regime, however, now the energy scale of the tunnel splitting is of the order of fractions of meV, i.e. from $10^{10}$to 10^{11} Hz. Here the INS lineshape of the energy gain and energy loss transitions are analyzed. They correspond to transitions between the singlet and triplet wavefunctions [19]. From this analysis the coherent tunnel frequency and the incoherent tunnel rates are determined and the spectral parameters J and k are elucidated. J determines the line position, k the increase in line width due to the presence of incoherent exchange.

As an experimental example of such an INS lineshape analysis, the INS spectra of the protonated isotopomer of the same tungsten dihydrogen complex $W(PCy_3)(CO)_3(\eta^2\text{-}H_2)$ are presented.

The superimposed experimental and calculated spectra are depicted in Fig. 21.21. Here the lineshape associated with the two rotational tunnel transitions of the complex is simulated as a function of the parameters J and k. For the sake of clarity, plots of the calculated line shapes of the outer rotational tunnel transitions without the contribution of the quasi-elastic center line are included. J increases only slightly with increasing temperature, in contrast to the Lorentzian line widths W which increase strongly. In other words, the lines broaden with increasing temperature until they disappear. One notes that the relative intensity of the singlet–triplet and the triplet–singlet transitions are almost the same over the whole temperature range covered, in contrast to the case of a thermal equilibrium between the singlet and the triplet states. This indicates that the singlet–triplet conversion rates are very slow in the sample measured, and that the actual relative intensity of the two peaks is arbitrarily dependent on the history of the sample.

21.4.2
Kinetic Data Obtained from the Experiments

The above described experiments allow determination of the coherent and incoherent dihydrogen exchange rates of the two complexes.

WILEY-VCH
Schowen
1. UK
N. Denzau

Kühn & Weyh Satz und Medien
Freiburg
l:/Vch/Schowen/3b2/c21.3d
19. 7. 2006

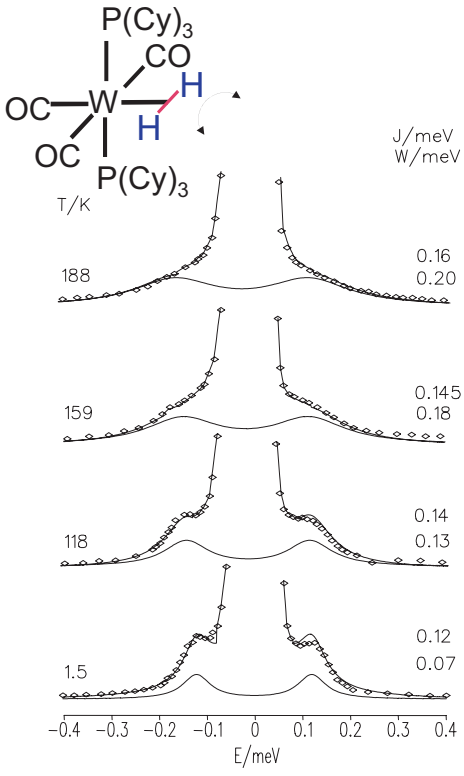

Figure 21.21 Superposed experimental and calculated INS spectra of $W(PCy)_2(CO)_3(\eta\text{-}H_2)$ as function of temperature (adapted from Refs. [19, 42, 97]). *W* is the total line width in meV; *J* is the rotational tunnel splitting in meV (1 meV = 2.318 ×10^{11} Hz = 8.065 cm^{-1}).

21.4.2.1 **Ru-D_2 Complex**

In the case of the Ru-D_2 complex the data from the lineshape analysis and the T_1-relaxation data are combined in Fig. 21.22 which shows an Arrhenius plot of the temperature dependence of X_{12} and k_{12}.

While the temperature dependence of X_{12} is very weak and nearly linear in the temperature window between 5 and 20 K, the incoherent exchange rate k_{12} exhibits a strong non-Arrhenius behavior and varies from 5×10^3 s^{-1} at 5.4 K to ca. 2.5×10^6 s^{-1} at 103 K and ca. 10^{11} s^{-1} at 300 K. The rate data from both types of experiments overlap between 20 K and 100 K and there is an excellent agreement between the values. This indicates that both rates result from the same motional process.

The simulation of the temperature dependence was performed assuming a thermally activated tunneling process, described by a Bell type of tunneling. The high temperature rate in the tunnel model was chosen as 4×10^{12} s^{-1}, which is expected from the Eyring equation. Since the observed increase in k_{12} at low temperatures is not obtainable by a simple one-dimensional Bell model an effective power law potential was employed:

$$V_{eff}(T^{-1}) = V(T_0^{-1}) + (V(T_1^{-1}) - V(T_0^{-1}))\left(\frac{T^{-1} - T_0^{-1}}{T_1^{-1} - T_0^{-1}}\right)^G \qquad (21.82)$$

WILEY-VCH
Schowen
1. UK
N. Denzau
Kühn & Weyh Satz und Medien
Freiburg
l:/Vch/Schowen/3b2/c21.3d
19. 7. 2006

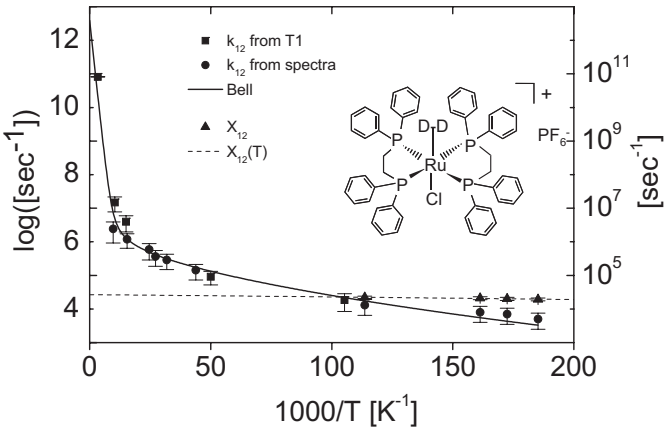

Figure 21.22 Arrhenius plot of the temperature dependence of the coherent tunneling and incoherent exchange rates in the Ru-D_2 sample (adapted from Ref. [40]), extracted from Fig. 21.18 and Fig. 21.19. The solid line is the result of a fit of the temperature dependence of the incoherent rates using a modified Bell tunnel model (see text). The dashed line is a simple linear fit of the coherent tunnel rates.

The best fit of the experimental rates (solid line in Fig. 21.22) was found for an exponent of $G = 0.7$. The effective potential varies between 268 meV(6.18 kcal mol^{-1}) at 5.4 K and 129 meV (2.97 kcal mol^{-1}) at 300 K. This effective potential gives a good reproduction of the experimental data. These rates were used to calculate the whole T_1 dependence (solid line in Fig. 21.19). Moreover there is an excellent agreement between the low temperature value of 268 meV and the value of 270 meV extracted from the ^{2}H NMR lineshape analysis.

This temperature dependent effective potential shows that a complete description of the temperature dependence of the rates needs at least a two-dimensional model, where the average R_{HH} and/or R_{RuH} distances are functions of the temperature.

21.4.2.2 W(PCy)3(CO)3 (η-H2) Complex

In the case of the W-H_2 complex NMR data from the deuterated complex and INS data from the protonated complex are available. This allows a comparison of the exchange rates and thus a determination of the H/D isotope effect of the reaction rate. For this the T_1 values from Fig. 20.21 are converted to rate constants of the D–D exchange and plotted together with the rate data of the H–H exchange from the INS spectra. The resulting curve (Fig. 21.23) shows a deviation from simple Arrhenius behavior at low temperatures. This deviation is evidence for the presence of a quantum mechanical tunneling process at low temperatures, similar to the tunneling observed in the Ru-D_2 sample. Comparison of these rate data with the H–H exchange rates determined from the lineshape analysis of the INS spectra of the protonated species reveals a strong isotope effect, which increases with lower temperatures.

WILEY-VCH
Schowen
1. UK
N. Denzau

Kühn & Weyh Satz und Medien
Freiburg
l:/Vch/Schowen/3b2/c21.3d
19. 7. 2006

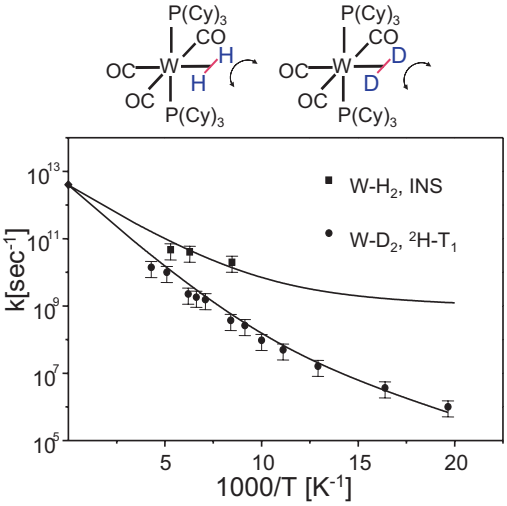

Figure 21.23 Arrhenius plot of the temperature dependence of the incoherent exchange rates in the W-D_2 sample, extracted from the ^2H T_1 data (adapted from Ref. [41]). The data are compared to data obtained on the W-H_2 complex, determined by INS. The solid lines are the results of fits of the temperature dependence of the incoherent rates using a Bell type tunnel model. The fits reveal a strong isotope effect, which is not solely attributable to a simple mass effect. The high temperature limit of the rates was chosen as 4×10^{12} s^{-1}, according to the Eyring equation.

Calculations with the Bell tunnel model reveal that this isotope effect is not solely explainable by the differences of the masses of the two hydrogen isotopes. Thus the activation energy must also have changed. This change in the activation barrier may be caused by isotope effects on the M–D and D–D versus M–H and H–H distances and/or by differences in the zero point energy of the ground or an activated state, which serves as the transition state for the tunneling. At low temperatures the latter is probably the major contribution to the strong isotope effect, since the quadrupolar coupling constant of the low temperature spectra (not shown) is practically constant at low temperatures.

21.5 Summary and Conclusion

This chapter presents some effects symmetry has on the rates and mechanisms of chemical reactions. The reaction kinetics of low mass groups like dihydrogen or dideuterium, in particular at low temperatures, is strongly influenced by quantum mechanical tunneling processes and the Fermi postulate of the symmetry of the

WILEY-VCH
Schowen
1. UK
N. Denzau
Kühn & Weyh Satz und Medien
Freiburg
l:/Vch/Schowen/3b2/c21.3d
19. 7. 2006

wavefunction. These effects are particularly clearly manifested in NMR spectra, where coherent tunnel processes are visible as line splitting and incoherent tunnel processes are visible as line broadenings or relaxation rates. The complex kinetics of a superimposed coherent and incoherent exchange on both INS and NMR lineshapes is describable via two simple, temperature dependent spectroscopic parameters J and k, which are measures of the tunnel splitting and the incoherent exchange rate.

Symmetry effects are also important for the diagnostic application of parahydrogen in para-hydrogen induced polarization (PHIP) effects. While the spinphysics of these isotopomers is well understood there is still a large field of possible applications. Probably the current biggest challenge in this field is the development of biophysical and medical applications of these spin-isotopomers. There the extremely high spin polarization could be employed for sensitivity enhancements in MRI or functional studies of hydrogenase and related enzymes.

Finally, we wish to note that hydrogen is not the only small molecule, where molecular exchange symmetry causes the existence of a para- and an ortho- spin isotopomer. Water is another important example. In the gas phase it exists as para- or ortho-water. They are distinguishable by IR. Their concentration ratio is used in astronomy as a remote temperature sensor. The spin conversion mechanisms of these isotopomers are still an open field for future studies [98, 99].

Acknowledgements

This research has been supported by the Deutsche Forschungsgemeinschaft, Bonn, and the Fonds der Chemischen Industrie (Frankfurt).

References

1 A. Farkas, *Orthohydrogen, Parahydrogen and Heavy Hydrogen*, Cambridge, 1935.
2 G. J. Kubas, R. R. Ryan, B. I. Swanson, P. J. Vergamini, H. J. Wasserman, *J. Am. Chem. Soc.* **116**, 451 (1984).
3 G. J. Kubas, *Acc. Chem. Res.* **21**, 120 (1988).
4 N. Aebischer, U. Frey, A. E. Merbach, *Chem.Comm.*, 2303 (1998).
5 G. Albertin, S. Antoniutti, S. Garciafontan, R. Carballo, F. Padoan, *J. Chem. Soc., Dalton Trans.*, 2071 (1998).
6 I. Alkorta, I. Rozas, J. Elguero, *Chem. Soc. Rev.* **27**, 163 (1998).
7 V. I. Bakhmutov, *Inorg. Chem.* **37**, 279 (1998).
8 T. Y. Bartucz, A. Golombek, A. J. Lough, P. A. Maltby, R. H. Morris, R. Ramachandran, M. Schlaf, *Inorg. Chem.* **37**, 1555 (1998).
9 M. G. Basallote, J. Duran, M. J. Fernandez-Trujillo, M. A. Manez, *J. Chem. Soc., Dalton Trans.*, 2205 (1998).
10 C. Bohanna, B. Callejas, A. J. Edwards, M. A. Esteruelas, F. J. Lahoz, L. A. Oro, N. Ruiz, C. Valero, *Organometallics*, 373 (1998).
11 G. Buntkowsky, H.-H. Limbach, F. Wehrmann, I. Sack, H. M. Vieth, R. H. Morris, *J. Phys. Chem. A* **101**, 4679 (1997).

WILEY-VCH
Schowen
1. UK
N. Denzau

Kühn & Weyh Satz und Medien
Freiburg
l:/Vch/Schowen/3b2/c21.3d
19. 7. 2006

12 B. Chaudret, *Coord. Chem. Rev.* **180**, 381 (1998).
13 A. C. Cooper, K. G. Caulton, *Inorg. Chem.* **37**, 5938 (1998).
14 R. H. Crabtree, *J. Organomet. Chem.* **557**, 111 (1998).
15 M. A. Esteruelas, L. A. Oro, *Chem. Rev.* **98**, 577 (1998).
16 R. Gelabert, M. Moreno, J. M. Lluch, A. Lledos, *J. Am. Chem. Soc.* **120**, 8168 (1998).
17 S. Gründemann, H.-H. Limbach, V. Rodriguez, B. Donnadieu, S. Sabo-Etienne, B. Chaudret, *Ber. Bunsenges. Phys. Chem.* **102**, 344 (1998).
18 T. Hasegawa, Z. W. Li, H. Taube, *Chem. Lett.*, 7 (1998).
19 H.-H. Limbach, S. Ulrich, S. Gründemann, G. Buntkowsky, S. Sabo-Etienne, B. Chaudret, G. J. Kubas, J. Eckert, *J. Am. Chem. Soc.* **120**, 7929 (1998).
20 K. S. Macfarlane, I. S. Thorburn, P. W. Cyr, D. Chau, S. J. Rettig, B. R. James, *Inorg. Chim. Acta* **270**, 130 (1998).
21 W. S. Ng, G. C. Jia, M. Y. Huang, C. P. Lau, K. Y. Wong, L. B. Wen, *Organometallics* **17**, 4556 (1998).
22 P. L. A. Popelier, *J. Phys. Chem. A* **102**, 1873 (1998).
23 S. Sabo-Etienne, B. Chaudret, *Chem. Rev.* **98**, 2077 (1998).
24 S. S. Stahl, J. A. Labinger, J. E. Bercaw, *Inorg. Chem.* **37**, 2422 (1998).
25 P. G. Jessop, R. H. Morris, *Coord. Chem. Rev.* **121**, 155 (1992).
26 D. M. Heinekey, W. J. Oldham, *J. Chem. Rev.* **93**, 913 (1993).
27 P. A. Maltby, M. Steinbeck, A. J. Lough, R. H. Morris, W. T. Klooster, T. F. Koetzle, R. C. Srivastava, *J. Am. Chem. Soc.* **118**, 5396 (1996).
28 T. A. Luther, D. M. Heinekey, *Inorg. Chem.* **37**, 127 (1998).
29 A. Toupadakis, G. J. Kubas, W. A. King, L. B. Scott, J. Huhmann-Vincent, *Organometallics* **17**, 5315 (1998).
30 S. Q. Niu, L. M. Thomson, M. B. Hall, *J. Am. Chem. Soc.* **121**, 4000 (1998).
31 M. E. Cucullu, S. P. Nolan, T. R. Belderrain, R. H. Grubbs, *Organometallics* **17**, 1299 (1998).
32 A. J. Lough, R. H. Morris, L. Ricciuto, T. Schleis, *Inorg. Chim. Acta* **270**, 238 (1998).
33 F. Maseras, A. Lledos, E. Clot, O. Eisenstein, *Chem. Rev.* **100**, 601 (2000).
34 J. Matthes, S. Grundemann, A. Toner, Y. Guari, B. Donnadieu, J. Spandl, S. Sabo-Etienne, E. Clot, H. H. Limbach, B. Chaudret, *Organometallics* **23**, 1424 (2004).
35 A. Macchioni, *Chem. Rev.* **105**, 2039 (2005).
36 S. Lachaize, W. Essalah, V. Montiel-Palma, L. Vendier, B. Chaudret, J. C. Barthelat, S. Sabo-Etienne, *Organometallics* **24**, 2935 (2005).
37 H. H. Limbach, G. Scherer, M. Maurer, B. Chaudret, *Angew. Chem., Int. Ed. Engl.* **31**, 1369 (1990).
38 H. H. Limbach, G. Scherer, M. Maurer, *Angew. Chem.* **104**, 1414 (1992).
39 H. H. Limbach, G. Scherer, L. Meschede, F. Aguilar-Parrilla, B. Wehrle, J. Braun, C. Hoelger, H. Benedict, G. Buntkowsky, W. P. Fehlhammer, J. Elguero, J. A. S. Smith, B. Chaudret, in *Ultrafast Reaction Dynamics and Solvent Effects, Experimental and Theoretical Aspects*, Y,.Gauduel, P.J. Rossky (Eds.), American Institute of Physics., New York 1993, p. 225.
40 F. Wehrmann, T. Fong, R. H. Morris, H.-H. Limbach, G. Buntkowsky, Phys. Chem. Chem. Phys. **1**, 4033 (1999).
41 F. Wehrmann, J. Albrecht, E. Gedat, G. J. Kubas, H. H. Limbach, G. Buntkowsky, *J. Phys. Chem. A* **106**, 2855 (2002).
42 J. Eckert, G. J. Kubas, *J. Phys. Chem.* **97**, 2378 (1993).
43 T. Arliguie, B. Chaudret, J. Devillers, R. Poilblanc, *C. R. Acad. Sci. Paris, Ser. I* **305**, 1523 (1987).
44 D. M. Heinekey, N. G. Payne, G. K. Schulte, *J. Am. Chem. Soc.* **110**, 2303 (1988).
45 D. M. Heinekey, J. M. Millar, T. F. Koetzle, N. G. Payne, K. W. Zilm, *J. Am. Chem. Soc.* **112**, 909 (1990).
46 K. W. Zilm, D. M. Heinekey, J. M. Millar, N. G. Payne, P. Demou, *J. Am. Chem. Soc.* **111**, 3088 (1989).

47 D. Jones, J. A. Labinger, J. Weitekamp, *J. Am. Chem. Soc.* **111**, 3087 (1989).
48 S. J. Inati, K. W. Zilm, *Phys. Rev. Lett.*, **68**, 3273 (1992).
49 M. T. Bautista, K. A. Earl, P. A. Maltby, R. H. Morris, C. T. Schweitzer, A. Sella, *J. Am. Chem. Soc.* **110**, 7031 (1988).
50 G. A. Facey, T. P. Fong, D. G. Gusev, P. M. MacDonald, R. H. Morris, M. Schlaf, W. Xu, *Can. J. Chem.* **1899–1910** (1999).
51 C. R. Bowers, D. P. Weitekamp, *Phys. Rev. Lett.* **57**, 2645 (1986).
52 T. C. Eisenschmidt, R. U. Kirss, P. P. Deutsch, S. I. Hommeltoft, R. Eisenberg, J. Bargon, *J. Am. Chem. Soc.* **109**, 8089 (1987).
53 G. Buntkowsky, B. Walaszek, A. Adamczyk, Y. Xu, H.-H. Limbach, B. Chaudret, *Phys. Chem. Chem. Phys.* **8**, 1929 (2006).
54 I. F. Silvera, *Rev. Mod. Phys.* **52**, 393 (1980).
55 J. van Kranendonk, *Solid Hydrogen*, Plenum, New York 1983.
56 C. R. Bowers, D. H. Jones, N. D. Kurur, J. A. Labinger, M. G. Pravica, D. P. Weitekamp, *Adv. Magn. Reson.* **15**, 269 (1990).
57 R. Eisenberg, T. C. Eisenschmid, M. S. Chinn, R. U. Kirss, *Adv. Chem. Ser. D*, 47 (1992).
58 S. B. Duckett, C. L. Newell, R. Eisenberg, *J. Am. Chem. Soc.* **116**, 10548 (1994).
59 J. Barkemeyer, M. Haake, J. Bargon, *J. Am. Chem. Soc.* **117**, 2927 (1995).
60 R. Eisenberg, *J. Chin. Chem. Soc.* **42**, 471 (1995).
61 M. Haake, J. Barkemeyer, J. Bargon, *J. Phys. Chem.* **99**, 17539 (1995).
62 G. Buntkowsky, J. Bargon, H.-H. Limbach, *J. Am. Chem. Soc.* **118**, 867 (1996).
63 M. Jang, S. B. Duckett, R. Eisenberg, *Organometallics* **15**, 2863 (1996).
64 S. B. Duckett, C. J. Sleigh, *Progr. NMR. Spectrosc.* **34**, 71 (1999).
65 J. Natterer, O. Schedletzky, J. Barkemeyer, J. Bargon, S. J. Glaser, *J. Magn. Reson.* **133**, 92 (1998).
66 H. G. Niessen, D. Schleyer, S. Wiemann, J. Bargon, S. Steines, B. Driessen-Hoelscher, *Magn. Reson. Chem.* **38**, 747 (2000).
67 S. M. Oldham, J. F. Houlis, C. J. Sleigh, S. B. Duckett, R. Eisenberg, *Organometallics* **19**, 2985 (2000).
68 A. Eichhorn, A. Koch, J. Bargon, *J. Mol. Catal. A* **174**, 293 (2001).
69 A. Koch, J. Bargon, *Inorg. Chem.* **40**, 533 (2001).
70 D. Schleyer, H. G. Niessen, J. Bargon, *New J. Chem.* **25**, 423 (2001).
71 S. Wildschutz, P. Hubler, J. Bargon, *Chem.Phys.Chem* **2**, 328 (2001).
72 D. C. Bregel, S. M. Oldham, R. Eisenberg, *J. Am. Chem. Soc.* **124**, 13827 (2002).
73 A. Permin, R. Eisenberg, *Inorg. Chem.* **41**, 2451 (2002).
74 M. Stephan, O. Kohlmann, H. G. Niessen, A. Eichhorn, J. Bargon, *Magn. Reson. Chem.* **40**, 157 (2002).
75 L. D. Vazquez-Serrano, B. T. Owens, J. M. Buriak, *Chem. Comm.*, 2518 (2002).
76 H. Johannesson, O. Axelsson, M. Karlsson, *Compt. Rend. Phys.* **5**, 315 (2004).
77 R. B. Bell, *The Tunnel Effect in Chemistry*, Chapman &Hall, London & New York 1980.
78 F. Hund, *Z. Phys.* **43**, 805 (1927).
79 F. A. Cotton, *Chemical Applications of Group Theory*, Wiley, New York 1963.
80 C. Cohen-Tannoudji, B. Diu, F. Laloe, *Mechanique Quantique*, Hermann Editeurs, Paris 1977.
81 G. Buntkowsky, *Structural and Dynamical Studies with Dipolar and Quadrupolar Solid State NMR*, Free University, Berlin 1999.
82 R. Ernst, G. Bodenhausen, A. Wokaun, *Principles of NMR in One and Two Dimensions,* Clarendon Press, Oxford 1987.
83 S. Szymanski, P. Bernatowicz, *Annu. Rev. NMR* **54**, 1 (2005).
84 S. Szymanski, *J. Chem. Phys.* **104**, 8216 (1996).
85 C. Scheurer, R. Wiedenbruch, R. Meyer, R. R. Ernst, D. M. Heinekey, *J. Chem. Phys.* **106**, 1 (1997).
86 G. Buntkowsky, unpublished results.
87 G. Gamow, *Z. Phys. Chem.* **51**, 204 (1927).

WILEY-VCH
Schowen
1. UK
N. Denzau

Kühn & Weyh Satz und Medien
Freiburg
l:/Vch/Schowen/3b2/c21.3d
19. 7. 2006

88 G. Gamow, *Z. Phys. Chem.* **52**, 510 (1928).
89 E. U. Condon, R. W. Gurney, *Nature* **112**, 439 (1928).
90 E. U. Condon, R. W. Gurney, *Phys. Rev.* **33**, 127 (1929).
91 G. Wentzel, *Z. Phys.* **138**, 518 (1926).
92 H. A. Kramers, *Z. Phys.* **39**, 828 (1926).
93 L. Brillouin, *C. R. Acad. Sci.* **153**, 24 (1926).
94 H. G. Niessen, C. Ulrich, J. Bargon, *J. Labelled Compd. Radiopharm.* **43**, 711 (2000).
95 S. Alexander, *J. Chem. Phys.* **37**, 971 (1962).
96 G. Binsch, *J. Am. Chem. Soc.* **91**, 1304 (1969).
97 J. Eckert, G. J. Kubas, A. J. Dianoux, *J. Chem. Phys.* **88**, 466 (1988).
98 V. I. Tikhonov, A. A. Volkov, *Science* **296**, 2363 (2002).
99 H. H. Limbach, G. Buntkowsky, J. Matthes, S. Gründemann, T. Pery, B. Walaszek, B. Chaudret, *Chem.Phys.Chem.*, in press (2006).

Author Queries Chapter 21

Please cite Figure 21.1 in the text.

You had 2 equation numbers (21.49) and (21.50) for one equation. I have renumbered ok?

Refs. 1, publisher?
99, update?
I deleted your ref. 75 as there is no need for a reference to the current book, a chapter number is sufficient.